Mitochondrial dysfunction leads to nuclear genome instability: A link through iron-sulfur clusters

Joshua R. Veatch[1], Michael A. McMurray[2], Zara W. Nelson and Daniel E. Gottschling*

Division of Basic Sciences, Fred Hutchinson Cancer Research Center and [1]the Molecular and Cellular Biology Program, University of Washington
Seattle, WA, USA

[2]Current address: Department of Molecular and Cell Biology, University of California at Berkeley, Berkeley, CA, USA

* Corresponding author.
Address: Fred Hutchinson Cancer Research Center
Mailstop A3-025
1100 Fairview Ave N
P.O. Box 19024
Seattle, WA, 98109
Phone: 206-667-4494
Fax: 206-667-5894
e-mail: dgottsch@fhcrc.org

Key words: Loss of heterozygosity, genome integrity, mitochondrial membrane potential, iron-sulfur cluster, *Saccharomyces cerevisiae*

SUMMARY

Mutations and deletions in the mitochondrial genome (mtDNA), as well as instability of the nuclear genome, are involved in multiple human diseases. Here we report that in *Saccharomyces cerevisiae*, loss of mtDNA leads to nuclear genome instability, through a process of cell cycle arrest and selection we define as a cellular crisis. This crisis is not mediated by the absence of respiration, but instead correlates with a reduction in the mitochondrial membrane potential. Analysis of cells undergoing this crisis identified a defect in iron-sulfur cluster (ISC) biogenesis, which requires normal mitochondrial function. We found that down-regulation of non-mitochondrial ISC protein biogenesis was sufficient to cause increased genomic instability in cells with intact mitochondrial function. These results suggest mitochondrial dysfunction stimulates nuclear genome instability by inhibiting the production of ISC-containing protein(s), which are required for maintenance of nuclear genome integrity.

INTRODUCTION

Nuclear genome instability, a hallmark of cancer, is thought in many cases to be an early event in tumorigenesis (Nowell, 1976). One form of genomic instability that plays an important role in tumor progression is loss of heterozygosity (LOH). In a heterozygous situation, where one functional dominant allele is "covering" the phenotype of a defective recessive allele, loss of the functional allele can have grave consequences and is frequently a means by which tumor suppressor genes are inactivated in cancer (Brown, 1997)

Normal mitochondrial function appears to be important for nuclear genome integrity. In yeast, defects in mitochondrial function are associated with increased levels of genetic change in the nuclear genome (Flury et al., 1976; Rasmussen et al., 2003), and reactive oxygen species originating in mitochondria are thought to be a major source of endogenous nuclear DNA damage (Huang and Kolodner, 2005). However, the connections between mitochondrial function and nuclear genome integrity are poorly understood.

Mitochondria are required for cellular energy production via oxidative phosphorylation, and the conserved processes of iron metabolism (Lill and Muhlenhoff, 2008), programmed cell death (Eisenberg et al., 2007), the production of reactive oxygen (Boveris et al., 1972), and intermediary metabolism (Jones and Fink, 1982). In both yeast and humans, the mtDNA encodes a small fraction of the ~1000 proteins that function in the mitochondria (Sickmann et al., 2003). In *Saccharomyces cerevisiae*, the mtDNA encodes components of the mitochondrial translational apparatus, as well as protein subunits of respiratory complexes III, IV and V (Contamine and Picard, 2000). These

proteins reside in the inner mitochondrial membrane, where they are involved in respiration and the formation of the electrochemical potential across the membrane. However, the nuclear genome encodes the remaining subunits of complexes III, IV and V (Tzagoloff and Dieckmann, 1990), and the proteins required for all other aspects of mitochondrial function (Sickmann et al., 2003). The nuclear-encoded gene products must be imported into the mitochondria post-translationally (Rehling et al., 2004).

The mtDNA is required for respiration, but is dispensable for the viability of budding yeast (Nagley and Linnane, 1970), and some human cell types (King and Attardi, 1989). Although the mtDNA is dispensable in these cases, the mitochondria themselves are essential for cell viability. The inner mitochondrial electrochemical membrane potential, which is required for mitochondrial protein import, biogenesis, and cellular viability, is normally maintained by respiration (Baker and Schatz, 1991). However, in both yeast and human cells that lack mtDNA, the membrane potential is maintained through hydrolysis of ATP by the nucleus-encoded F_1 subunit of ATP synthase (Buchet and Godinot, 1998; Giraud and Velours, 1997; Kominsky et al., 2002).

One essential function of the mitochondria is the synthesis of iron-sulfur clusters (ISCs), which serve catalytic and structural functions in many cellular proteins (Lill and Muhlenhoff, 2008). The initial reactions that assemble ISCs on protein scaffolds occur in the mitochondrial matrix, and they are subsequently incorporated into mitochondrial ISC-containing proteins, or exported from the mitochondria for insertion into cytoplasmic and nuclear ISC-containing proteins (Lill and Muhlenhoff, 2008). Thus, assembly of all ISC-containing proteins requires intact mitochondria in both yeast (Kispal et al., 1999) and humans (Biederbick et al., 2006).

It has been known for many years that the loss of expression from the mtDNA in yeast results in pleiotropic phenotypes that are not completely explained by the loss of respiration (Dujon, 1981). Specifically, cells that lack, or have severely rearranged, mtDNA display different mitochondrial morphologies (Church and Poyton, 1998), as well as different genetic requirements for viability (Kotylak and Slonimski, 1977) than respiration deficient cells with intact mtDNA. These observations suggest that loss of function of the mtDNA could affect mitochondrial pathways other than respiration.

Previously, we described the phenomenon of age-associated LOH in *S. cerevisiae* in which a dramatic increase of genome instability occurs with delayed onset, during the pedigree analysis of yeast mother cells (McMurray and Gottschling, 2003). Here we present evidence that the LOH we observed is the result of mitochondrial dysfunction, and we provide an explanation for how these two events are linked.

RESULTS

Mitochondrial dysfunction correlates with LOH events in pedigree analysis of individual yeast cells

In an earlier study using pedigree analysis, we reported an age-associated increase in LOH in the budding yeast *S. cerevisiae* (McMurray and Gottschling, 2003). Starting with naive mother cells, all the daughter cells produced by a single mother are allowed to form colonies. LOH at heterozygous marker genes located at the distal ends of chromosomes XII and IV are then detected by colony color phenotypes: LOH events that occur during the growth of colonies are visible as colored sectors in the colonies. We reported a striking increase in the number of LOH events occurring after ~25 mother cell

divisions, manifested as an increased frequency of colonies with greater than 1/8 sector of colony color.

In order to better understand the basis for this increase in LOH, we further characterized the colonies with LOH and discovered that many showed evidence of mitochondrial dysfunction. These colonies were small (Figure 1A) and were unable to respire (data not shown). In an examination of 40 mother cells, these colonies, known as "petites" (Ephrussi and Slonimski, 1955), occurred later in the lifespan of the mother. Most long lived mother cells eventually gave rise to daughters that exclusively formed either petite colonies or were unable to form colonies (Figure S1 A & B). The most common spontaneous events that result in mitochondrial dysfunction in budding yeast are either mtDNA rearrangements [ρ^-], or total loss of the mtDNA [ρ^0], which prevent the production of mitochondria-encoded proteins (Dujon, 1981). We mated these respiratory-deficient cells from seven independent pedigrees to a respiratory-deficient ρ^0 strain (data not shown). The resulting cells failed to respire, indicating that the respiratory deficiency of the petite colonies was due to a lesion in the mtDNA (Stevens, 1981).

The nature of the mtDNA lesion was characterized by examining cytoplasmic DNA staining (Stevens, 1981) in the petite daughter colonies from 15 different pedigrees (Figure S1C). We found that the majority of petite colonies were entirely comprised of cells without mtDNA [ρ^0] (89%, 114/128), and the remaining 11% of colonies contained a mix of cells with and without mtDNA [ρ^-]. Thus, mitochondrial dysfunction in pedigree analysis occured through damage to or loss of the mitochondrial genome.

It was evident that most nuclear LOH events occurred in colonies that also had mitochondrial dysfunction (Figure 1A, Figure S1A & B). Specifically, the frequency of

LOH events for loci on either chromosome XII or IV (Figure 1B) was much greater in colonies with mitochondrial dysfunction compared to those with normal mitochondria. These results indicated that an increase in LOH correlated with mitochondrial dysfunction and that LOH was not further impacted by the number of cell divisions that the mother cell had undergone (Figure 1B). This suggested that mitochondrial dysfunction leads to increased LOH in the nuclear genome.

Loss of mtDNA leads to nuclear genome instability

In order to test whether loss of mtDNA could lead to LOH in the nuclear genome, mtDNA was eliminated by two independent methods. First, a dominant-negative mutation was created in the *S. cerevisiae* nuclear-encoded mitochondrial DNA polymerase gene, *MIP1* (Foury, 1989; Jazayeri et al., 2003). This dominant negative allele ($MIP1^{DN}$) was placed under control of a promoter that allowed it to be induced by addition of estradiol (Gao and Pinkham, 2000). Expression of the $MIP1^{DN}$ allele for 6-7 hours caused rapid and complete loss of the mtDNA from cells, as measured by the absence of DAPI staining in the cytoplasm (Figure S2 (Stevens, 1981)) and their inability to respire (data not shown). Strikingly, the petite colonies that formed after the transient expression of $MIP1^{DN}$ displayed a very large number of nuclear LOH events at the chromosome XII and IV loci (Figure 1C & D).

Similar results were obtained by a second method for eliminating mtDNA. Cells were exposed to a transient low-dose treatment of ethidium bromide, a cationic, lipophilic DNA-intercalating agent that preferentially eliminates mtDNA (Ferguson and von Borstel, 1992). Colonies that formed after the ethidium bromide pulse had highly elevated levels of LOH events on chromosomes IV and XII (Figure 1C & D). LOH

events following mtDNA loss by either treatment were found to be due to recombination, not chromosome loss or locus specific mutation (Figure S3). Taken together, these results indicate that loss of mtDNA leads to nuclear genome instability.

Loss of mtDNA leads to a progressive growth defect and cell cycle arrest

In addition to exhibiting LOH, we noticed that the petite colonies were highly variable in size, whether arising spontaneously in the pedigree analysis or due to either of the treatments mentioned above (Figures 1A & C). We investigated this heterogeneity further, to determine whether there was any relationship between colony size and the observed increase in LOH. Cell growth was analyzed immediately after mtDNA elimination by ethidium bromide treatment or expression of the *MIP1*^{DN} allele. Cells were analyzed under dilute culture conditions so that they did not enter into the diauxic shift or stationary phase (DeRisi et al., 1997). The newly created ρ^0 cells initially divided at a rate similar to ρ^+ cells (75 minutes vs 66 minutes per doubling, respectively), but this was followed by a progressive slowing of growth such that after 30 hours, the culture doubled once every ~400 minutes (Figure 2A & B). This was in marked contrast to ρ^+ cells, which retained a rapid doubling time.

A slow growth rate in culture could result from a high frequency of cell death, cell cycle arrest, and/or a slower cell cycle. In order to distinguish between these possibilities, individual cells were micromanipulated onto plates at different times after mtDNA loss. Immediately after mtDNA loss, nearly all cells divided and formed colonies (Figure 3C). However, over time, more and more cells could not form colonies (Figure 3C). By 22 hours, 60% of the cells in these cultures were permanently arrested as unbudded cells (Figure 3C) and had a G_1 DNA content (Figure S4). Interestingly, these arrested cells

were metabolically active even after 30 hours, as measured by their ability to exclude the vital dye phloxine B (Figure S4) (Severin and Hyman, 2002). Thus, at least part of the progressive slowing in culture growth rate following loss of mtDNA results from a gradual accumulation of G_1 arrested cells. This suggests that after actively growing cells lose their mtDNA, many of the cells arrest, while those that go on to divide display high levels of nuclear genome instability.

Spontaneous genetic changes suppress inviability of cells lacking mtDNA

Colonies that did form from cells following loss of mtDNA were of variable size, and repeated passaging of cells resulted in clones that showed improved growth despite the continued absence of the mtDNA (data not shown). These clones remained unable to respire and grew slower than cells with intact mtDNA, but they formed colonies more readily, grew faster, and displayed fewer nuclear LOH events than cells within the first 30 hours following loss of their mtDNA (data not shown). This suggested that the cells made compensations for the loss of the mtDNA to achieve improved growth and relatively stable nuclear genomes.

To test whether the compensation was the result of genetic changes in the nuclear genome, haploid cells were transiently treated with ethidium bromide, which caused the same kinetics of slow growth and increased number of arrested cells as seen in the diploid cells described above (data not shown). Four independent haploid clones that arose showing stronger growth were selected for further analysis. These cells were crossed to an isogenic partner strain with intact mtDNA, the diploid was sporulated, and the meiotic progeny were analyzed for growth after eliminating mtDNA. In all four cases, the ability to grow well in the absence of the mtDNA segregated as either one nuclear

locus (three cases – Figure S5) or two unlinked loci (one case – Figure S5). Four of five suppressor alleles were recessive and each recessive allele complemented the others in a diploid, indicating that they were in different nuclear genes (data not shown). Each of these spontaneous suppressor alleles showed improved growth during the ~40 hours following mtDNA loss, relative to wild-type cells (Figure 2D; three single locus suppressors are displayed), though each had a different kinetic growth profile following mtDNA elimination. Taken together, these observations indicate that following loss of mtDNA, there is a progressive loss of viability and a selection for nuclear mutations that improve growth in the absence of mtDNA. During this process, there is a large increase in the frequency of recombination events in the nuclear genome. We define this phenomenon of progressive slow growth, cell cycle arrest, and nuclear genomic instability, as the "crisis" that follows the loss of mtDNA.

The crisis following mtDNA loss is not a general consequence of respiratory deficiency

We next asked whether the crisis observed upon mtDNA loss was a consequence of respiratory deficiency. To address this question deletions in three different nuclear genes required for respiration at different steps of the electron transport chain were made. Cat5 is required for the synthesis of Coenzyme Q, which transfers electrons to complex III (Jonassen et al., 1998), Rip1 is an integral component of electron chain complex III (Lange and Hunte, 2002), and Cox4 is required for the function of electron transport complex IV (Koerner et al., 1985). Consistent with previous reports, we found that there was no defect in growth in any of these three respiratory mutants (Figure 3B-D), despite the fact that each one eliminates the ability to respire (Francis et al., 2007). In addition,

none of the mutants had increased LOH events compared to wild type cells (Figure 3A). Yet, after eliminating the mtDNA, each mutant behaved like the wild-type and experienced the crisis marked by a progressive growth decline and increased nuclear LOH (Figure 3A-D). These observations showed that respiratory deficiency was not sufficient to cause the crisis nor increased LOH, and suggested that loss of the mtDNA has additional effects beyond eliminating the ability to respire.

Loss of the inner mitochondrial membrane electrochemical potential correlates with the crisis

In addition to loss of respiration, the loss of mtDNA in mammalian (Jazayeri et al., 2003) or yeast cells (Dunn and Jensen, 2003; Pringle et al., 1989) results in a reduction of the inner mitochondrial membrane electrochemical potential ($\Delta\Psi$). This potential is required for the import of proteins into the mitochondrial matrix in all cells (Schleyer et al., 1982). In respiring cells the $\Delta\Psi$ is normally generated through the reactions of electron transport and oxidative phosphorylation. But in ρ^0 cells, these reactions do not occur due to the absence of complex III, IV and the F_0 component of ATP synthase. Instead, it is thought that $\Delta\Psi$ is generated through the efforts of the mitochondrial adenine nucleotide translocator and the F_1 ATP synthase, both of which are encoded by the nuclear genome (Dupont et al., 1985; Giraud and Velours, 1997; Kominsky et al., 2002). However, this alternate mode appears to produce a lower $\Delta\Psi$ than that achieved through electron transport and oxidative phosphorylation in ρ^+ cells (Dupont et al., 1985).

We hypothesized that reduction in the $\Delta\Psi$ contributed to the crisis after loss of mtDNA. We tested this idea by examining ρ^0 cells carrying a mutation that increases $\Delta\Psi$.

The *ATP1-111* allele encodes a hyperactive F_1 ATP synthase that generates a larger $\Delta\Psi$ in ρ^0 cells than wild-type cells do when they are ρ^0 (Francis et al., 2007). When mtDNA was eliminated from *ATP1-111/ATP1-111* diploid cells there was no detectable crisis, as was evident by robust growth (Figure 4A), the absence of cell cycle arrest (data not shown) and reduced nuclear LOH (Figure 4B). Thus, the *ATP1-111* allele prevented the crisis upon mtDNA loss, suggesting that a reduction in $\Delta\Psi$ does indeed contribute to the crisis.

To obtain additional evidence for the importance of $\Delta\Psi$ in the crisis, a cell biological assay was carried out with the various alleles described above. Consistent with previous reports (Dunn and Jensen, 2003; Pringle et al., 1989), we found that the mitochondria of cells with no mtDNA stain less brightly with $DiOC_6$ (Figure S6), which concentrates in the mitochondrial matrix, based on the magnitude of the inner mitochondrial membrane potential (Pringle et al., 1989). However, we noticed that there was less cellular uptake of the dye into these cells (Figure S6). Therefore, as a second approach to assess $\Delta\Psi$ *in vivo,* we examined the import of fluorescently tagged proteins into the mitochondrial matrix (Swayne et al., 2007). Nuclear-encoded proteins that go into the matrix require $\Delta\Psi$ (Schleyer et al., 1982). By contrast, outer mitochondrial membrane proteins do not depend on the inner mitochondrial membrane potential for their localization (Gasser and Schatz, 1983). We used a chimeric fusion protein containing the inner mitochondrial membrane targeting pre-sequence of Cox4 and mCherry, a monomeric red fluorescent protein (preCox4-Cherry) (Shaner et al., 2004) as a reporter for matrix targeted protein, and a fusion of the outer mitochondrial membrane protein Tom70 with green fluorescent protein (Tom70-GFP).

In cells with intact mtDNA, preCox4-Cherry co-localized to reticular structures with Tom70-GFP as expected (Figure 4C). But in cells with no mtDNA, preCox4-Cherry showed diffuse cytoplasmic localization. While the structure of the mitochondria, as shown by Tom70-GFP localization, was altered in these cells, the Tom70-GFP still localized to discrete sub-cellular structures (Figure 4C).

Similar to the crisis following the loss of the mtDNA, impaired protein import is not a general consequence of respiratory deficiency, because mitochondrial localization of preCox4-Cherry was not altered in cells that are unable to respire due to deletions of *CAT5*, *RIP1* or *COX4* (Figure S7). Furthermore, the *ATP1-111* mutation significantly increased the number of cells with mitochondrial localization of preCox4-Cherry; it went from 12% (7/41 cells) in *ATP1* ρ^0 cells to 67% (44/66 cells) in *ATP1-111* ρ^0 cells ($p < 0.0001$, Figure 4C). This is consistent with the *ATP1-111* mutation increasing $\Delta\Psi$ in ρ^0 cells, and that it is this increase in $\Delta\Psi$ that prevents the crisis following mtDNA loss. Taken together, these data suggest that there is a reduction in $\Delta\Psi$ following the loss of mtDNA, and that this leads to the cellular crisis, which includes increased nuclear genomic instability.

Loss of mtDNA leads to a transcriptional signature of iron starvation

We also employed expression profiling as an independent approach to understand the relationship between mitochondrial dysfunction and LOH. Expression array analysis revealed that a large number of genes were differentially expressed 27 hours after mtDNA loss: 313 genes were up-regulated and 174 genes were down-regulated more than 2-fold (Table S1). The group of genes most highly affected matched the transcriptional signature of iron starvation (Puig et al., 2005). Up-regulated genes were

enriched for genes involved in iron assimilation that are induced in iron starvation conditions by the transcription factors Aft1 and Aft2 (16 of 18 genes, $p=7.1x10^{-19}$, Figure 5) (Puig et al., 2005). Down-regulated genes were enriched for iron-dependent genes whose messages are degraded during iron starvation (16 of 34 genes, $p=4.63x10^{-16}$, Figure 5). Slight induction of a subset of the iron regulon occurred as early as 3 hours after mtDNA loss, but maximal induction of most genes did not occur until 24 hours later.

Iron sensing in yeast is mediated by the acquisition of iron from the environment (Puig et al., 2005), successful packaging of iron into iron-sulfur clusters in the mitochondria (Rutherford et al., 2005), and the export of ISCs from the mitochondria to the cytosol (Kispal et al., 1997). Cytoplasmic ISCs act as a signal to keep the iron regulon transcription factors Aft1 and Aft2 in the cytoplasm (Rutherford et al., 2005). Thus defects in iron availability or import, mitochondrial ISC biogenesis or mitochondrial ISC export, or Aft1/Aft2 localization could all potentially lead to an iron starvation response. We propose that the iron starvation response following mtDNA loss results from defects in mitochondrial iron import, ISC biogenesis, or ISC export, based on the following observations. First, loss of the mtDNA increased total cellular iron (Figure S8C), indicating that iron availability and import are not the cause of this response. Second, the expression profile of cells 27 hours following loss of the mtDNA closely resemble those of cells defective in mitochondrial ISC biosynthesis when an essential protein in this process, Yah1, is depleted (Hausmann et al., 2008) ($p=7.6x10^{-82}$ for overlap of genes up-regulated $\geq$ 2 fold, $p=1.3x10^{-43}$ for overlap of genes downregulated $\geq$ 2-fold, Figure 5), or when export of ISCs from the mitochondria to the cytoplasm is reduced through

depletion of the transport protein Atm1 (Hausmann et al., 2008) ($p=1.9x10^{-31}$ for overlap of genes upregulated $\geq$ 2-fold, $p=3.0x10^{-25}$ for overlap of genes downregulated $\geq$ 2-fold, Figure 5). Third, restored mitochondrial protein import with the *ATP1-111/ ATP1-111* mutation largely suppressed activation of the iron regulon following loss of the mtDNA. Twenty-seven hours after mtDNA loss, the induction of the iron regulon in *ATP1-111/ ATP1-111* cells most closely resembled that of wild-type cells 11 hours after they lost their mtDNA – before the crisis occurred (Figure 5). This suggests that the defect responsible for iron regulon induction is mitochondrial in origin. Finally, others have observed that mitochondrial ISC biogenesis is impaired in cells lacking mtDNA (Kaut et al., 2000), and in cells lacking a mitochondrial membrane potential (Kispal et al., 1999). Taken together, these observations indicate that loss of the mtDNA leads to a defect in mitochondrial iron metabolism, and that this plays a role in causing the crisis and nuclear genome instability.

Increased intracellular iron levels are not required for the crisis or nuclear genome instability that follows mtDNA loss

Impaired ISC biogenesis has two major consequences for the cell. First, there is activation of the iron regulon, which increases iron uptake and leads to increased levels of free intracellular iron (Kispal et al., 1997; Kispal et al., 1999). Second, the function of ISC-containing proteins in both the mitochondrial compartment and throughout the cell is either reduced or lost. These proteins are involved in various mitochondrial, nuclear and cytoplasmic processes (Lill and Muhlenhoff, 2008). Because elevated levels of free iron can lead to cell cycle abnormalities (Philpott et al., 1998) and oxidative damage to biomolecules, including protein and DNA (Karthikeyan et al., 2002; Karthikeyan et al.,

2003), we tested whether elevated cellular iron levels were responsible for the crisis that followed mtDNA loss. Cellular iron was increased following mtDNA loss (Figure S8C), and there was a commensurate increase in oxidative damage to cellular protein (Figure S8A), as has been previously observed with elevated iron in a mitochondrial ISC mutant (Karthikeyan et al., 2003).

To test whether this increase in cellular iron and oxidative damage was responsible for the crisis and the LOH following mtDNA loss, the *AFT1* gene was deleted. *AFT1* encodes a major activator of the iron regulon; without it, increases in iron uptake from the environment are abrogated (Yamaguchi-Iwai et al., 1995). As expected, *aft1*Δ cells did not experience an increase in cellular iron (Figure S8C), nor was there an increase in global protein oxidation, following loss of mtDNA (Figure S8B). However, the increase in nuclear LOH and slow growth following mtDNA loss persisted in *aft1*Δ cells (Figure S8D & E), though the kinetics of reduced growth rate (Figure S8E) and cell cycle arrest (data not shown) were slower compared to wild-type cells. This argues that while increased iron and oxidative damage may play a role in the crisis following mtDNA loss, they are not required for the increased nuclear genomic instability that occurs during the crisis. Therefore, the nuclear genomic instability following mtDNA loss could be a direct consequence of reduced function of ISC-containing proteins, rather than indirect consequences that follow iron regulon activation.

Reduced function of cytoplasmic/nuclear ISC biogenesis leads to increased nuclear genome instability

Given these results, we next wanted to test whether loss of function in cellular ISC-containing proteins, occurring as a consequence of mtDNA loss, caused nuclear

genomic instability. To this end we constructed an allele that allowed us to directly control ISC insertion into cytoplasmic and nuclear proteins. Repression of the *NAR1* gene only alters packaging of ISCs into non-mitochondrial proteins (Balk et al., 2004) without inducing the iron regulon (Rutherford et al., 2005) or altering ISC insertion into mitochondrial proteins (Balk et al., 2004). *NAR1* is an essential gene, so we controlled its expression using the estradiol-inducible described above. When cells were switched from medium with high estradiol, where Nar1 is expressed, into medium with low levels of estradiol, where Nar1 is repressed, the culture showed a progressive decline in growth rate over the course of 24 hours (data not shown). Unlike cells that lost their mtDNA, these cells did not arrest in the G1 stage of the cell cycle (data not shown). However, colonies formed by these cells on low estradiol medium display an increased incidence of LOH in the nuclear genome at both chromosomes tested (Figure 6A & B), despite the fact that mitochondrial function remains intact (data not shown). Consistent with previous reports, we find that the iron regulon is not activated with reduced *NAR1* function (Figure 5) (Hausmann et al., 2008; Rutherford et al., 2005). These results show that reduced function of non-mitochondrial ISC containing proteins can cause nuclear genomic instability and suggest that loss or reduced function of these proteins plays a role in the crisis following loss of mtDNA. Other aspects of the crisis, such as G1-specific arrest, are likely to be mediated by additional, unknown processes that are affected by the loss of mtDNA.

DISCUSSION

Mitochondrial dysfunction leads to nuclear genome instability

We initially observed that nuclear genomic instability occurred with delayed onset in the pedigree analysis of individual cells (McMurray and Gottschling, 2003). Here we show that this increase in nuclear LOH is the result of damage to, and/or loss of, the mtDNA (Figure 1). Thus we have divided the phenomenon of age-associated LOH into at least two steps. First, cells lose mtDNA function over time – by a process that remains unknown – and second, the mtDNA loss results in a crisis that ultimately leads to increased nuclear genome LOH – which is the focus of this report.

The loss of the mtDNA in rich medium with glucose leads to a cellular crisis that is manifested as a gradual reduction in growth rate, cell cycle arrest, and increased nuclear genome instability (Figures 1 and 2). Of the cells that "adapted" to the crisis, it appears that most, if not all, of the cells harbored altered nuclear genomes. This is supported by two observations: the amount of LOH was extremely high, even though only two independent loci from the entire genome were monitored; and greater than 25% of colonies had large sectors indicative of an LOH event at either of the loci (Figure 2). Secondly, viable clones arose that carried nuclear mutations allowing them to survive (Figures 2 and S5).

Several years after the discovery that cytoplasmically inherited mutations could alter mitochondrial function (Ephrussi et al., 1949), a phenomenon was described in yeast cells with "extra-nuclear respiratory" mutations (James and Spencer, 1958). We believe this phenomenon to be the crisis following mtDNA loss that we report here. These mutants showed a loss of growth along with selection for nuclear mutations that allowed cells to survive (James and Spencer, 1958). We propose that our work now provides an explanation for these earlier observations. However, part of our work contrasts with more

recent studies that conducted expression analysis of cells lacking mtDNA: they did not observe activation of the iron regulon that we saw (Epstein et al., 2001; Traven et al., 2001). We examined cells a short amount of time after mtDNA loss, whereas the other studies did not examine the cells until they had been passaged for many generations without mtDNA. Furthermore, there appears to be a number of genetic modifiers of the crisis that could also explain differences between studies (JRV and DEG, unpublished data); derivatives of the common lab strain S288C – which is the basis of the systematic gene-deletion mutant collection (Giaever et al., 2002) – were used in our study, while different strains were used in the other studies.

Linking mtDNA loss to nuclear genome instability: A cascade involving iron-sulfur clusters

We propose the following model to explain the connection between mtDNA damage and nuclear genomic instability we have found. In normal cells, iron sulfur clusters (ISCs) are formed in the mitochondria through the action of multiple nucleus-encoded proteins. Some of these ISCs are exported to the cytoplasm, where they repress inappropriate activation of the iron regulon and function in multiple proteins, including several known to be involved in nuclear genome maintenance (Figure 7A). Following mtDNA loss or damage, a reduction in the mitochondrial membrane potential leads to decreased protein import into the mitochondria, leading to a defect in either iron import into the mitochondria, ISC packaging in the mitochondria, or ISC export into the cytosol. This leads to activation of the iron regulon and decreased function of cellular ISC containing proteins (Figure 7B). The finding that repressed non-mitochondrial ISC packaging resulted in nuclear genome instability in the absence of iron regulon activation (Figure

7C) suggests that a primary defect in the function of these proteins explained the connection between mitochondrial dysfunction and the integrity of the nuclear DNA. It is notable that the repression of ISC biogenesis does not explain all aspects of the crisis following mtDNA loss, in particular the G1 specific arrest. Other mechanisms, associated with loss of respiration and/or iron regulon induction, may be responsible for these other phenotypes.

The full complement of ISC-containing proteins in *S. cerevisiae* is unknown. Nevertheless, there are several nuclear genome integrity proteins that contain ISCs. These include Rad3, a helicase involved in nucleotide-excision repair (Rudolf et al., 2006); Pri2, a primase involved in lagging strand DNA synthesis and important in DNA double-strand break repair (Klinge et al., 2007); and Ntg2, a glycosylase involved in base-excision repair (Alseth et al., 1999). Future efforts may determine whether loss of mtDNA reduces the *in vivo* enzymatic activity of one or more of these candidate proteins, or yet to be identified proteins, to generate the increased LOH phenotype. However, if the activity of all three of these candidate proteins were attenuated, it could explain the high rate of genomic instability observed, as three DNA repair pathways would be compromised simultaneously.

Consequences of mtDNA damage: beyond the electron transport chain

Mitochondrial dysfunction and damage to the mtDNA is thought to play a role in many pathologies, and is proposed to be a driving force behind the aging process (Kujoth et al., 2007; Wallace, 2005). To explain the link between mitochondrial dysfunction and reduced cellular function, much attention has focused on the respiratory aspects of mitochondria – i.e., the electron transport chain – and its role in producing energy, or in

generating reactive oxygen species that can damage biomolecules (Dimauro and Davidzon, 2005; Wallace, 2005). The crisis that includes nuclear genome instability following mtDNA loss is not likely due to changes in respiration: mutations that simply block steps in electron transport and oxidative phosphorylation do not produce increased LOH (Figure 4).

Another mitochondrial pathway connected to the electron transport chain and implicated in genome instability is programmed cell death, which has been reported to occur in yeast (Eisenberg et al., 2007), and is largely dependent upon the yeast caspase homolog *MCA1* (Madeo et al., 2002). When *MCA1* was deleted, neither the decline in growth rate nor the increase in nuclear LOH frequency following mtDNA loss were affected (Figure S9), suggesting that programmed cell death pathways are not involved in the crisis.

Another implication of our findings is that not all means of eliminating electron transport and oxidative phosphorylation are the same with respect to overall mitochondrial function, as has been observed several times before in yeast (Church and Poyton, 1998; Dagsgaard et al., 2001; Zhang and Moye-Rowley, 2001). Specifically, we find that elimination of complex III or IV, which completely block respiration, did not produce the crisis phenotype. Our results suggest that, in addition to its role in supporting respiration, some feature of the mtDNA is involved in maintaining mitochondrial function in the absence of respiration. Consistent with previous models (Dupont et al., 1985), we speculate that the components of the F_0 ATP synthase complex encoded in the mtDNA carry out this function.

Further implications

We hypothesize that cells which survive the crisis pass through a hypermutable state, as has been reported in bacteria and eukaryotic cells that are placed under stressful conditions (reviewed in (Galhardo et al., 2007)). The stress we note in our study is initiated with mitochondrial dysfunction and manifests as nuclear genome instability. Genetically altered survivors that arise following mitochondrial dysfunction return to relatively normal levels of genome instability (data not shown).

What aspects of our findings could extend beyond budding yeast to human disease? The mitochondrial membrane potential of human cells is also reduced following the loss of mtDNA (Jazayeri et al., 2003). Additionally, both the essential role of the mitochondria in ISC biogenesis (Biederbick et al., 2006), and the role of ISC-containing proteins in nuclear genome stability, are conserved (Alseth et al., 1999; Klinge et al., 2007; Rudolf et al., 2006). We speculate that non-respiratory functions of the mitochondria, including ISC biogenesis, could play a role in human disease that occurs as a consequence of mtDNA damage.

EXPERIMENTAL PROCEDURES

Strain and plasmid construction

All strains used in this study and their genotypes are presented in Table S2 and all oligonucleotides used in plasmid and strain constructions are listed in Table S3. Plasmid and allele constructions are provided in supplemental materials.

Loss of heterozygosity assay

Log phase grown cells were treated either with 30 μg/ml ethidium bromide, 1μM estradiol, or no treatment in YEPD and grown for 6-7 hours. The cells were then centrifuged, washed once with fresh medium, and grown in log phase for another 12-14 hours before plating ~200 cells/plate onto YEPD. Colonies were replicated to medium containing 0.1% lead nitrate (Cost and Boeke, 1996) after 5-7 days. All experiments were done in triplicate or quadruplicate, and all replicates behaved similarly. Confidence intervals of 95% were calculated by the Poisson distribution using data pooled from all replicates.

Growth rate measurements

Log phase cells were treated as described above in YEPD and grown for 6-7 hours. Growth rates of cultures were measured by optical density at 660 nm in 96-well plates using a Powerwave XS plate reader (BioTek, Winooski, VT). In each experiment, each curve represents the mean of at least 3 independent cultures, plus or minus the standard deviation.

Microscopy

All microscopy was carried out with a DeltaVision system (Applied Precision, LLC., Issaquah, WA) which has an Olympus IX70 inverted microscope equipped with a 100X/1.40 objective. Images were deconvoluted using Softworx 3.4.3.

Cells were grown and treated as described above for 6 hours followed by washing in fresh medium, and 15 hours of growth in YEPD, and fixed. TOM70-GFP was visualized with the FITC filter. PreCOX4-Cherry was visualized with the RD-TR-PE filter. Twenty z-stacks were taken at an interval of 0.3 μm, and the resulting images were deconvoluted and projected onto one plane using the brightest point at each x,y position.

Microarrays

RNA expression arrays were carried out as previously described (Gardner et al., 2005) using cultures grown in YEPD medium to an OD_{600} of about 1.0 in biological triplicate. Array data was normalized and analyzed using Genespring version 7.2 (Agilent). Heat maps were generated using Java Treeview (Saldanha, 2004).

ACKNOWLEDGMENTS

We thank F. Foury, P. Thorsness, J. Pinkham, R. Lill, R. Tsien and the Yeast Resource Center for reagents. We thank R. Lill and P. Thorsness for experimental advice, J. Vazquez for help with microscopy, and J. Delrow and R. Basom for help with expression array analysis. Thanks to members of the Gottschling lab for critical reading of this manuscript. This work was supported by fellowships to J.R.V. from a Genetic Approaches to Aging Training Grant (T32 AG00057) and the ARCS foundation, and FHCRC pilot project and National Institutes of Health grants (AG023779 & GM43893) to D.E.G.

Figure 1: Loss or damage to the mtDNA results in nuclear genomic instability. (A-B) Forty mother cells were analyzed by pedigree analysis. (A) left: Colonies produced by the 1st through 37th daughter of a single representative mother cell are shown (daughter 13 did not produce a colony). Right: The colonies from the left were replicated to media containing lead nitrate, which permits colony color development. Chromosome IV LOH results in a brown color, and chromosome XII LOH results in a red color. (B) The fraction of colonies that had at least a 1/8 sector of colony color are presented as a function of the number of cell divisions the mother cell went through. The data were classified as to whether the colony was normal or petite. Data are shown for LOH events that occurred on either the right arm of chromosome XII or IV. The difference in the LOH frequency between petite and normal cells for divisions 11-30 had a significance of $p<0.0001$ from chromosome XII and $p<0.001$ for chromosome IV.

(C) A wild-type (WT) strain was treated with or without a transient pulse of ethidium bromide (EtBr), and colonies grown from these cells were transferred to medium allowing visualization of LOH events. A derivative of the wild-type strain containing the dominant negative P_{GAL1}-$MIP1^{DN}$ allele under control of the Gal4-EBD-VP16 (GEV) fusion protein was treated with or without a transient pulse of estradiol (E2), and grown as described above. (D) The treatments described in C were carried out on the WT strain or derivatives of this strain that contain the GEV activator, and/or the dominant negative P_{GAL1}-$MIP1^{DN}$ as indicated. The percentage of colonies showing at least a 1/8 sector of LOH on chromosome XII and IV are presented. All error bars represent 95% confidence intervals and were calculated using the Poisson distribution.

Figure 2: Loss of the mtDNA leads to a progressive decline in growth rate, cell cycle arrest, and selection for suppressor clones. (A) Growth rate of isogenic strains containing the GEV transcriptional activator, P_{GAL1}-$MIP1^{DN}$ or both, following transient treatment with estradiol (E2). (B) Growth rate of the wild-type strain treated with or without a transient pulse of ethidium bromide. (C) The percentage of cells from (A) and (B) able to form a colony of at least 1mm in diameter after 8 days is presented on the left. The percentage of cells arrested as unbudded cells is presented on the right. Error bars represent 95% confidence intervals calculated using the binomial distribution. (D) Spontaneous [ρ^0] haploid suppressor mutants were back-crossed to isogenic cells with intact mtDNA. After sporulation, haploid [ρ^+] progeny of these crosses containing each suppressor allele were treated transiently with ethidium bromide and the growth rate was monitored as before.

Figure 3: The absence of respiration is not sufficient to cause the crisis and LOH. (A) Wild-type cells (UCC1899) and derivatives with homozygous deletions for either *COX4*, *RIP1* or *CAT5* were treated as described in Figure 2A. (B-D) Growth rate of cells with or without transient treatment with ethidium bromide. Wild-type cells are compared to deletions of *CAT5* (B), *RIP1* (C) or *COX4* (D).

Figure 4: A hyperactive F_1 ATP synthase partially restores mitochondrial protein import and prevents the growth defect and nuclear genomic instability that results from mtDNA loss. (A) Growth rates of a wild-type diploid and a the *ATP1-111/ATP1-111* derivative, with or without transient ethidium bromide treatment . (B) The frequency

of LOH events in the strains from (A). (C) Localization of proteins to the outer mitochondrial membrane (Tom70-GFP, green) or the mitochondrial matrix (preCox4-Cherry, red) in wild-type cells or *ATP1-111/ATP1-111* derivative cells are presented.

Figure 5: Cells show a transcriptional signature of iron starvation following mtDNA loss. Levels of mRNA from WT cells 3, 11, 19 and 27 hours after mtDNA loss were compared to cells with intact mtDNA. mRNA from *ATP1-111* mutants collected 27 hours after mtDNA loss was compared to mRNA of the same strain with intact mtDNA. mRNA was isolated from the *NAR1* repressible strain 27 hours after a shift from 50 nM estradiol to 2 nM estradiol and compared to the same strain grown in 50 nM estradiol. Genes are arranged in order of their reported magnitude of induction (red) or repression (green) by iron starvation (Puig et al., 2005). Comparisons are made to published array data for depletion of the *YAH1* and *ATM1* genes (Hausmann et al., 2008).

Figure 6: Reducing ISC protein loading activity in the cytoplasm leads to nuclear genome instability. (A) A strain (UCC3970) with *NAR1* expression controlled by estradiol (E2) was plated to media containing either 50 nM (*NAR1* expressed) or 2 nM estradiol (*NAR1* down-regulated) followed by replication to LOH indicator media. (B) The frequency of colonies showing at least 1/8 sector of LOH following plating of the strain in A ($NAR1^{EST}$) and an isogenic strain without the estradiol regulated promoter (WT) to either low (2nM) or high (50nM) estradiol (E2). Error bars represent 95% confidence intervals calculated using the Poisson distribution.

Figure 7: Model to explain nuclear genomic instability following mtDNA loss. A) In normal cells, iron is packaged into iron-sulfur clusters (ISCs) in the mitochondria, and some ISCs are exported into the cytoplasm. The cytoplasmic ISCs inhibit iron regulon induction and are required for the function of proteins that maintain nuclear genome integrity. (B) Upon loss of the mtDNA, the mitochondrial membrane potential ($\Delta\Psi$) is reduced, which compromises mitochondrial iron import, ISC packaging, and/or export. This results in iron regulon induction and nuclear genome instability. (C) Artificially reduced Nar1 function limits packaging of ISCs into proteins involved in nuclear DNA metabolism, leading to nuclear genome instability. In this case mitochondrial function is intact and the iron regulon is not induced.

REFERENCES

Alseth, I., Eide, L., Pirovano, M., Rognes, T., Seeberg, E., and Bjoras, M. (1999). The Saccharomyces cerevisiae homologues of endonuclease III from Escherichia coli, Ntg1 and Ntg2, are both required for efficient repair of spontaneous and induced oxidative DNA damage in yeast. Mol Cell Biol *19*, 3779-3787.

Baker, K.P., and Schatz, G. (1991). Mitochondrial proteins essential for viability mediate protein import into yeast mitochondria. Nature *349*, 205-208.

Balk, J., Pierik, A.J., Netz, D.J., Muhlenhoff, U., and Lill, R. (2004). The hydrogenase-like Nar1p is essential for maturation of cytosolic and nuclear iron-sulphur proteins. Embo J *23*, 2105-2115.

Biederbick, A., Stehling, O., Rosser, R., Niggemeyer, B., Nakai, Y., Elsasser, H.P., and Lill, R. (2006). Role of human mitochondrial Nfs1 in cytosolic iron-sulfur protein biogenesis and iron regulation. Mol Cell Biol *26*, 5675-5687.

Boveris, A., Oshino, N., and Chance, B. (1972). The cellular production of hydrogen peroxide. Biochem J *128*, 617-630.

Brown, M.A. (1997). Tumor suppressor genes and human cancer. Adv Genet *36*, 45-135.

Buchet, K., and Godinot, C. (1998). Functional F1-ATPase essential in maintaining growth and membrane potential of human mitochondrial DNA-depleted rho degrees cells. J Biol Chem *273*, 22983-22989.

Church, C., and Poyton, R.O. (1998). Neither respiration nor cytochrome c oxidase affects mitochondrial morphology in Saccharomyces cerevisiae. J Exp Biol *201*, 1729-1737.

Contamine, V., and Picard, M. (2000). Maintenance and integrity of the mitochondrial genome: a plethora of nuclear genes in the budding yeast. Microbiol Mol Biol Rev *64*, 281-315.

Cost, G.J., and Boeke, J.D. (1996). A useful colony colour phenotype associated with the yeast selectable/counter-selectable marker MET15. Yeast *12*, 939-941.

Dagsgaard, C., Taylor, L.E., O'Brien, K.M., and Poyton, R.O. (2001). Effects of anoxia and the mitochondrion on expression of aerobic nuclear COX genes in yeast: evidence for a signaling pathway from the mitochondrial genome to the nucleus. J Biol Chem *276*, 7593-7601.

DeRisi, J.L., Iyer, V.R., and Brown, P.O. (1997). Exploring the metabolic and genetic control of gene expression on a genomic scale. Science *278*, 680-686.

Dimauro, S., and Davidzon, G. (2005). Mitochondrial DNA and disease. Ann Med *37*, 222-232.

Dujon, B. (1981). Mitochondrial genetics and functions (Cold Spring Harbor, New York, Cold Spring Harbor Laboratory).

Dunn, C.D., and Jensen, R.E. (2003). Suppression of a defect in mitochondrial protein import identifies cytosolic proteins required for viability of yeast cells lacking mitochondrial DNA. Genetics *165*, 35-45.

Dupont, C.H., Mazat, J.P., and Guerin, B. (1985). The role of adenine nucleotide translocation in the energization of the inner membrane of mitochondria isolated from rho + and rho degree strains of Saccharomyces cerevisiae. Biochem Biophys Res Commun *132*, 1116-1123.

Eisenberg, T., Buttner, S., Kroemer, G., and Madeo, F. (2007). The mitochondrial pathway in yeast apoptosis. Apoptosis *12*, 1011-1023.

Ephrussi, B., Hottinguer, H., and Tavlitzki, J. (1949). Action de l'acriflovine sur les levures. II-Etude genetique de mutant "petite colonie.". Ann Inst Pasteur *77*, 419-450.

Epstein, C.B., Waddle, J.A., Hale, W.t., Dave, V., Thornton, J., Macatee, T.L., Garner, H.R., and Butow, R.A. (2001). Genome-wide responses to mitochondrial dysfunction. Mol Biol Cell *12*, 297-308.

Ferguson, L.R., and von Borstel, R.C. (1992). Induction of the cytoplasmic 'petite' mutation by chemical and physical agents in Saccharomyces cerevisiae. Mutat Res *265*, 103-148.

Flury, F., von Borstel, R.C., and Williamson, D.H. (1976). Mutator activity of petite strains of Saccharomyces cerevisiae. Genetics *83*, 645-653.

Foury, F. (1989). Cloning and sequencing of the nuclear gene MIP1 encoding the catalytic subunit of the yeast mitochondrial DNA polymerase. J Biol Chem *264*, 20552-20560.

Francis, B.R., White, K.H., and Thorsness, P.E. (2007). Mutations in the Atp1p and Atp3p subunits of yeast ATP synthase differentially affect respiration and fermentation in Saccharomyces cerevisiae. J Bioenerg Biomembr *39*, 127-144.

Galhardo, R.S., Hastings, P.J., and Rosenberg, S.M. (2007). Mutation as a stress response and the regulation of evolvability. Crit Rev Biochem Mol Biol *42*, 399-435.

Gao, C.Y., and Pinkham, J.L. (2000). Tightly regulated, beta-estradiol dose-dependent expression system for yeast. Biotechniques *29*, 1226-1231.

Gardner, R.G., Nelson, Z.W., and Gottschling, D.E. (2005). Degradation-mediated protein quality control in the nucleus. Cell *120*, 803-815.
Gasser, S.M., and Schatz, G. (1983). Import of proteins into mitochondria. In vitro studies on the biogenesis of the outer membrane. J Biol Chem *258*, 3427-3430.
Giaever, G., Chu, A.M., Ni, L., Connelly, C., Riles, L., Veronneau, S., Dow, S., Lucau-Danila, A., Anderson, K., Andre, B.*, et al.* (2002). Functional profiling of the Saccharomyces cerevisiae genome. Nature *418*, 387-391.
Giraud, M.F., and Velours, J. (1997). The absence of the mitochondrial ATP synthase delta subunit promotes a slow growth phenotype of rho- yeast cells by a lack of assembly of the catalytic sector F1. Eur J Biochem *245*, 813-818.
Hausmann, A., Samans, B., Lill, R., and Muhlenhoff, U. (2008). Cellular and mitochondrial remodeling upon defects in iron-sulfur protein biogenesis. J Biol Chem *283*, 8318-8330.
Huang, M.E., and Kolodner, R.D. (2005). A biological network in Saccharomyces cerevisiae prevents the deleterious effects of endogenous oxidative DNA damage. Mol Cell *17*, 709-720.
James, A.P., and Spencer, P.E. (1958). The Process of Spontaneous Extranuclear Mutation in Yeast. Genetics *43*, 317-331.
Jazayeri, M., Andreyev, A., Will, Y., Ward, M., Anderson, C.M., and Clevenger, W. (2003). Inducible expression of a dominant negative DNA polymerase-gamma depletes mitochondrial DNA and produces a rho0 phenotype. J Biol Chem *278*, 9823-9830.
Jonassen, T., Proft, M., Randez-Gil, F., Schultz, J.R., Marbois, B.N., Entian, K.D., and Clarke, C.F. (1998). Yeast Clk-1 homologue (Coq7/Cat5) is a mitochondrial protein in coenzyme Q synthesis. J Biol Chem *273*, 3351-3357.
Jones, E.W., and Fink, G.R. (1982). Regulation of Amino Acid and Nucleotide Biosynthesis in Yeast. In The Molecular Biology of the Yeast Saccharomyces: Metabolism and Gene Expression J. Strathern, Broach, ed. (Cold Spring Harbor, NY, Cold Spring Harbor Laboratory), pp. 181-299.
Karthikeyan, G., Lewis, L.K., and Resnick, M.A. (2002). The mitochondrial protein frataxin prevents nuclear damage. Hum Mol Genet *11*, 1351-1362.
Karthikeyan, G., Santos, J.H., Graziewicz, M.A., Copeland, W.C., Isaya, G., Van Houten, B., and Resnick, M.A. (2003). Reduction in frataxin causes progressive accumulation of mitochondrial damage. Hum Mol Genet *12*, 3331-3342.
Kaut, A., Lange, H., Diekert, K., Kispal, G., and Lill, R. (2000). Isa1p is a component of the mitochondrial machinery for maturation of cellular iron-sulfur proteins and requires conserved cysteine residues for function. J Biol Chem *275*, 15955-15961.
King, M.P., and Attardi, G. (1989). Human cells lacking mtDNA: repopulation with exogenous mitochondria by complementation. Science *246*, 500-503.
Kispal, G., Csere, P., Guiard, B., and Lill, R. (1997). The ABC transporter Atm1p is required for mitochondrial iron homeostasis. FEBS Lett *418*, 346-350.
Kispal, G., Csere, P., Prohl, C., and Lill, R. (1999). The mitochondrial proteins Atm1p and Nfs1p are essential for biogenesis of cytosolic Fe/S proteins. Embo J *18*, 3981-3989.

Klinge, S., Hirst, J., Maman, J.D., Krude, T., and Pellegrini, L. (2007). An iron-sulfur domain of the eukaryotic primase is essential for RNA primer synthesis. Nat Struct Mol Biol *14*, 875-877.
Koerner, T.J., Homison, G., and Tzagoloff, A. (1985). Nuclear mutants of Saccharomyces cerevisiae with altered subunits 4, 5, and 6 of cytochrome oxidase. J Biol Chem *260*, 5871-5874.
Kominsky, D.J., Brownson, M.P., Updike, D.L., and Thorsness, P.E. (2002). Genetic and biochemical basis for viability of yeast lacking mitochondrial genomes. Genetics *162*, 1595-1604.
Kotylak, Z., and Slonimski, P.P. (1977). Mitochondrial mutants isolated by a new screening method based upon the use of the nuclear mutation op1 (Berlin, Germany, Walter de Gruyter & Co.).
Kujoth, G.C., Bradshaw, P.C., Haroon, S., and Prolla, T.A. (2007). The role of mitochondrial DNA mutations in mammalian aging. PLoS Genet *3*, e24.
Lange, C., and Hunte, C. (2002). Crystal structure of the yeast cytochrome bc1 complex with its bound substrate cytochrome c. Proc Natl Acad Sci U S A *99*, 2800-2805.
Lill, R., and Muhlenhoff, U. (2008). Maturation of Iron-Sulfur Proteins in Eukaryotes: Mechanisms, Connected Processes, and Diseases. Annu Rev Biochem.
Madeo, F., Herker, E., Maldener, C., Wissing, S., Lachelt, S., Herlan, M., Fehr, M., Lauber, K., Sigrist, S.J., Wesselborg, S.*, et al.* (2002). A caspase-related protease regulates apoptosis in yeast. Mol Cell *9*, 911-917.
McMurray, M.A., and Gottschling, D.E. (2003). An age-induced switch to a hyper-recombinational state. Science *301*, 1908-1911.
Nagley, P., and Linnane, A.W. (1970). Mitochondrial DNA deficient petite mutants of yeast. Biochem Biophys Res Commun *39*, 989-996.
Nowell, P.C. (1976). The clonal evolution of tumor cell populations. Science *194*, 23-28.
Philpott, C.C., Rashford, J., Yamaguchi-Iwai, Y., Rouault, T.A., Dancis, A., and Klausner, R.D. (1998). Cell-cycle arrest and inhibition of G1 cyclin translation by iron in AFT1-1(up) yeast. Embo J *17*, 5026-5036.
Pringle, J.R., Preston, R.A., Adams, A.E., Stearns, T., Drubin, D.G., Haarer, B.K., and Jones, E.W. (1989). Fluorescence microscopy methods for yeast. Methods Cell Biol *31*, 357-435.
Puig, S., Askeland, E., and Thiele, D.J. (2005). Coordinated remodeling of cellular metabolism during iron deficiency through targeted mRNA degradation. Cell *120*, 99-110.
Rasmussen, A.K., Chatterjee, A., Rasmussen, L.J., and Singh, K.K. (2003). Mitochondria-mediated nuclear mutator phenotype in Saccharomyces cerevisiae. Nucleic Acids Res *31*, 3909-3917.
Rehling, P., Brandner, K., and Pfanner, N. (2004). Mitochondrial import and the twin-pore translocase. Nat Rev Mol Cell Biol *5*, 519-530.
Rudolf, J., Makrantoni, V., Ingledew, W.J., Stark, M.J., and White, M.F. (2006). The DNA repair helicases XPD and FancJ have essential iron-sulfur domains. Mol Cell *23*, 801-808.
Rutherford, J.C., Ojeda, L., Balk, J., Muhlenhoff, U., Lill, R., and Winge, D.R. (2005). Activation of the iron regulon by the yeast Aft1/Aft2 transcription factors depends

on mitochondrial but not cytosolic iron-sulfur protein biogenesis. J Biol Chem *280*, 10135-10140.

Saldanha, A.J. (2004). Java Treeview--extensible visualization of microarray data. Bioinformatics *20*, 3246-3248.

Schleyer, M., Schmidt, B., and Neupert, W. (1982). Requirement of a membrane potential for the posttranslational transfer of proteins into mitochondria. Eur J Biochem *125*, 109-116.

Severin, F.F., and Hyman, A.A. (2002). Pheromone induces programmed cell death in S. cerevisiae. Curr Biol *12*, R233-235.

Shaner, N.C., Campbell, R.E., Steinbach, P.A., Giepmans, B.N., Palmer, A.E., and Tsien, R.Y. (2004). Improved monomeric red, orange and yellow fluorescent proteins derived from Discosoma sp. red fluorescent protein. Nat Biotechnol *22*, 1567-1572.

Sickmann, A., Reinders, J., Wagner, Y., Joppich, C., Zahedi, R., Meyer, H.E., Schonfisch, B., Perschil, I., Chacinska, A., Guiard, B.*, et al.* (2003). The proteome of Saccharomyces cerevisiae mitochondria. Proc Natl Acad Sci U S A *100*, 13207-13212.

Stevens, B. (1981). Mitochondrial Structure (Cold Spring Harbor, New York, Cold Spring Harbor Laboratory).

Swayne, T.C., Gay, A.C., and Pon, L.A. (2007). Visualization of mitochondria in budding yeast. Methods Cell Biol *80*, 591-626.

Traven, A., Wong, J.M., Xu, D., Sopta, M., and Ingles, C.J. (2001). Interorganellar communication. Altered nuclear gene expression profiles in a yeast mitochondrial dna mutant. J Biol Chem *276*, 4020-4027.

Tzagoloff, A., and Dieckmann, C.L. (1990). PET genes of Saccharomyces cerevisiae. Microbiol Rev *54*, 211-225.

Wallace, D.C. (2005). A mitochondrial paradigm of metabolic and degenerative diseases, aging, and cancer: a dawn for evolutionary medicine. Annu Rev Genet *39*, 359-407.

Yamaguchi-Iwai, Y., Dancis, A., and Klausner, R.D. (1995). AFT1: a mediator of iron regulated transcriptional control in Saccharomyces cerevisiae. Embo J *14*, 1231-1239.

Zhang, X., and Moye-Rowley, W.S. (2001). Saccharomyces cerevisiae multidrug resistance gene expression inversely correlates with the status of the F(0) component of the mitochondrial ATPase. J Biol Chem *276*, 47844-47852.

Figure 1

Click here to download high resolution image

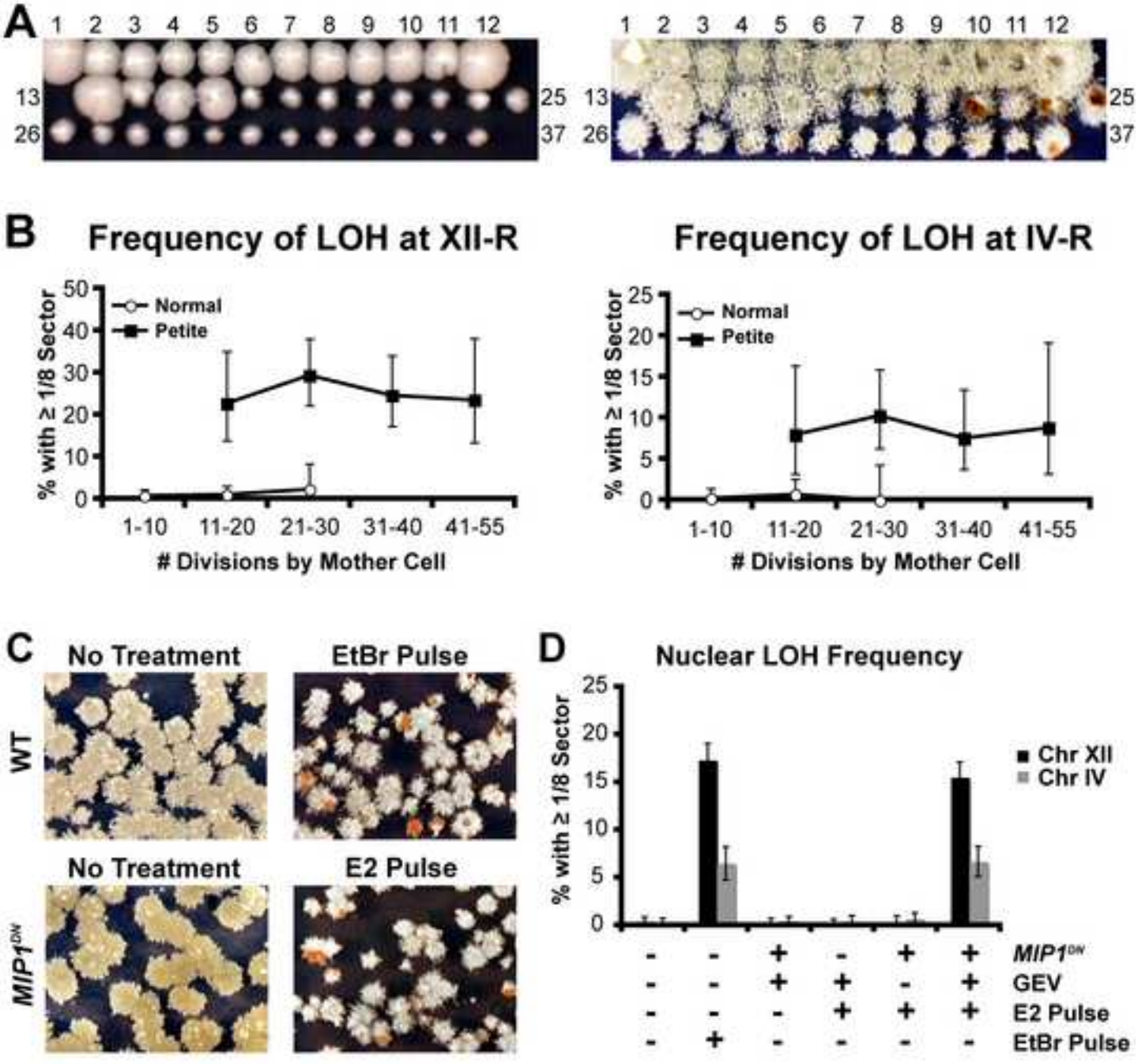

Figure 1

Figure 2

Click here to download high resolution image

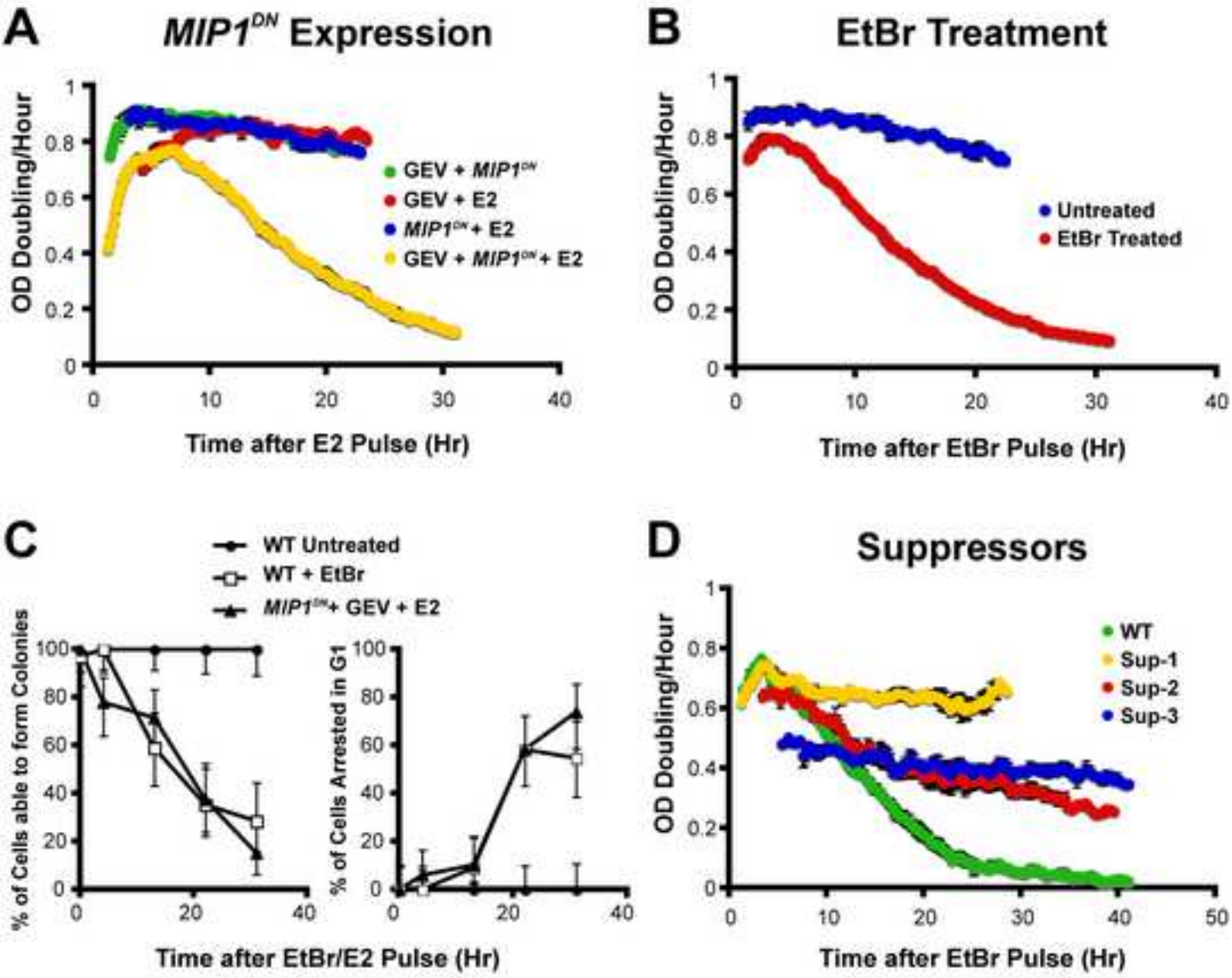

Figure 2

Figure 3

Click here to download high resolution image

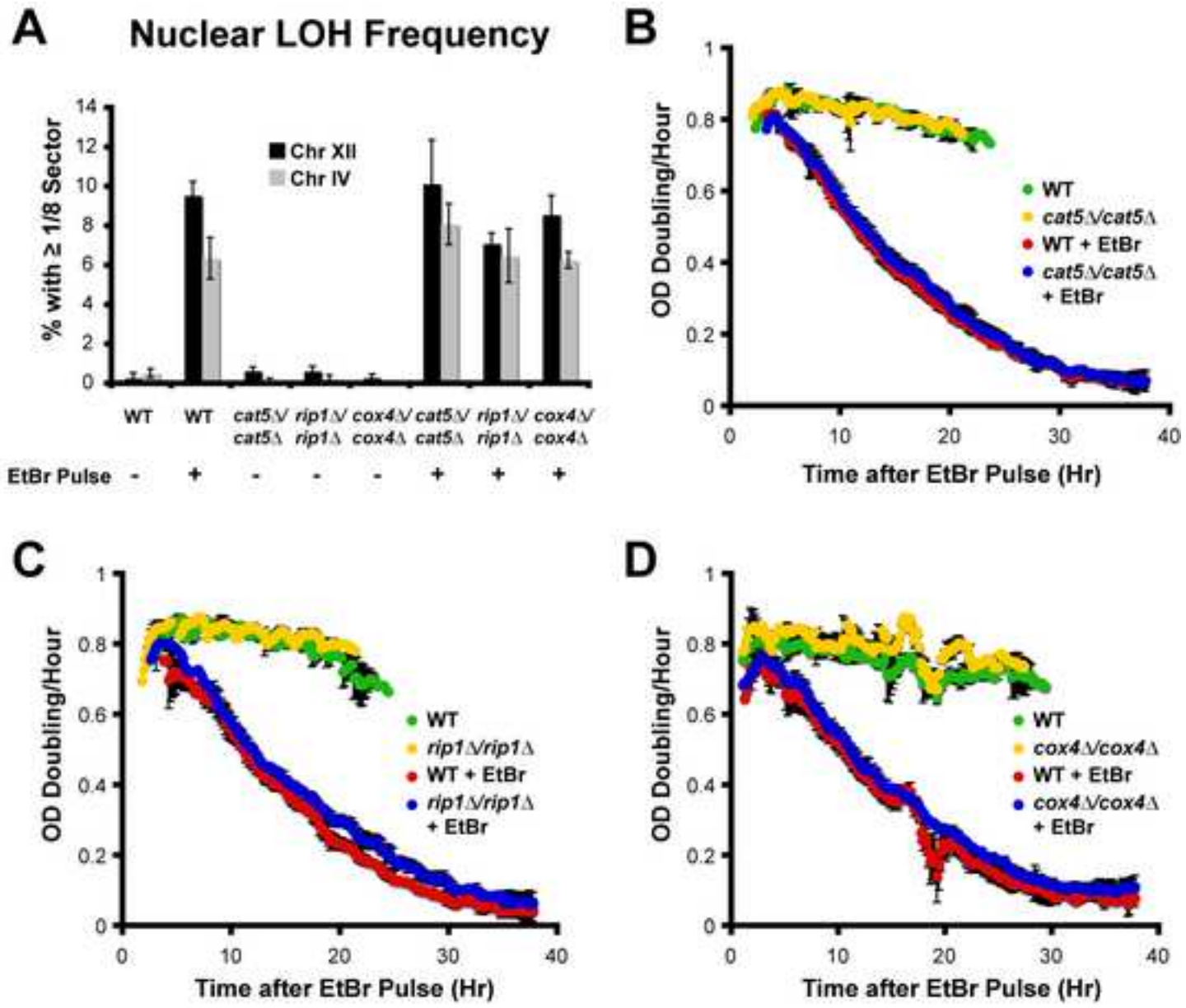

Figure 3

Figure 4

Click here to download high resolution image

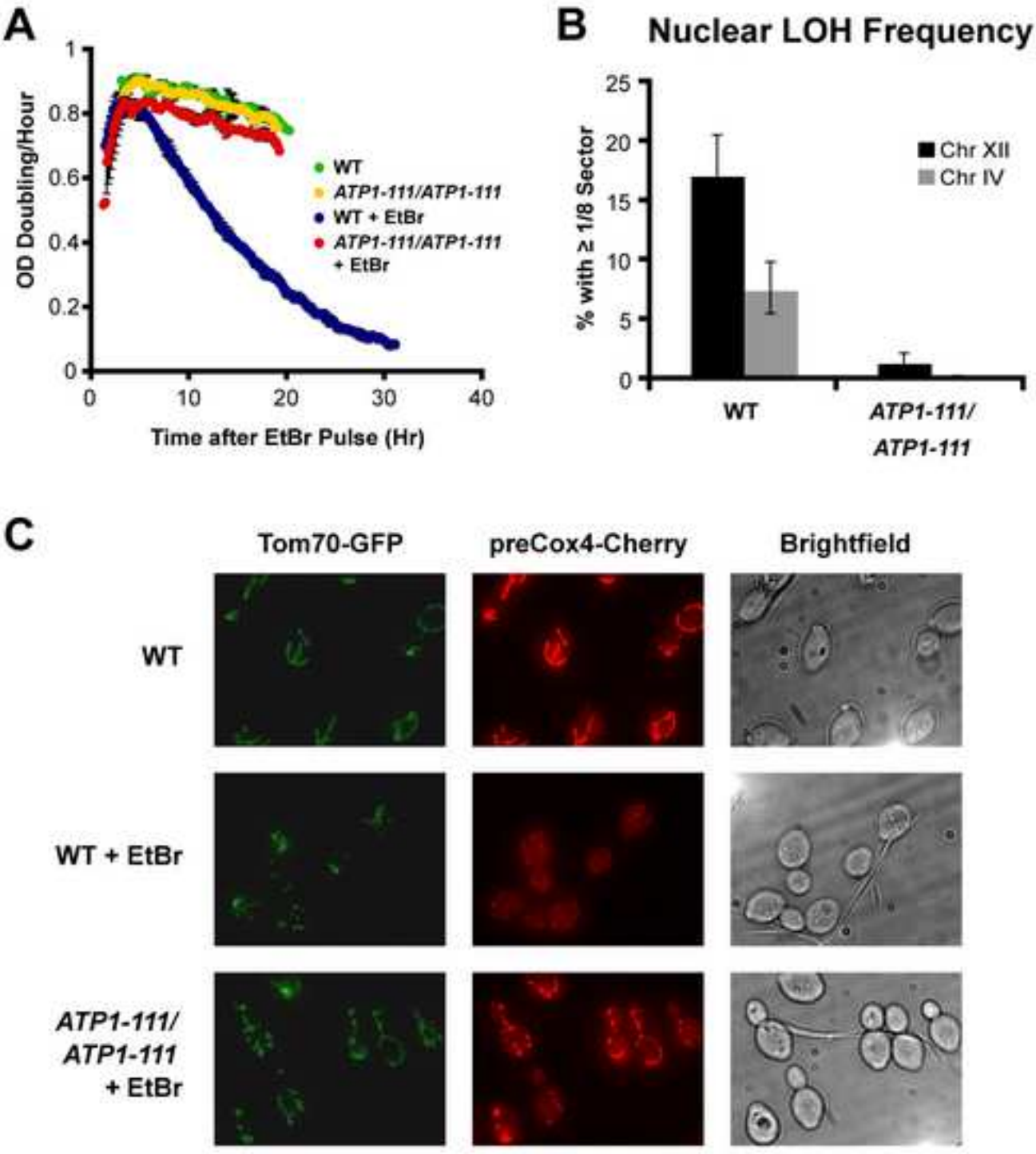

Figure 4

Figure 5

Click here to download high resolution image

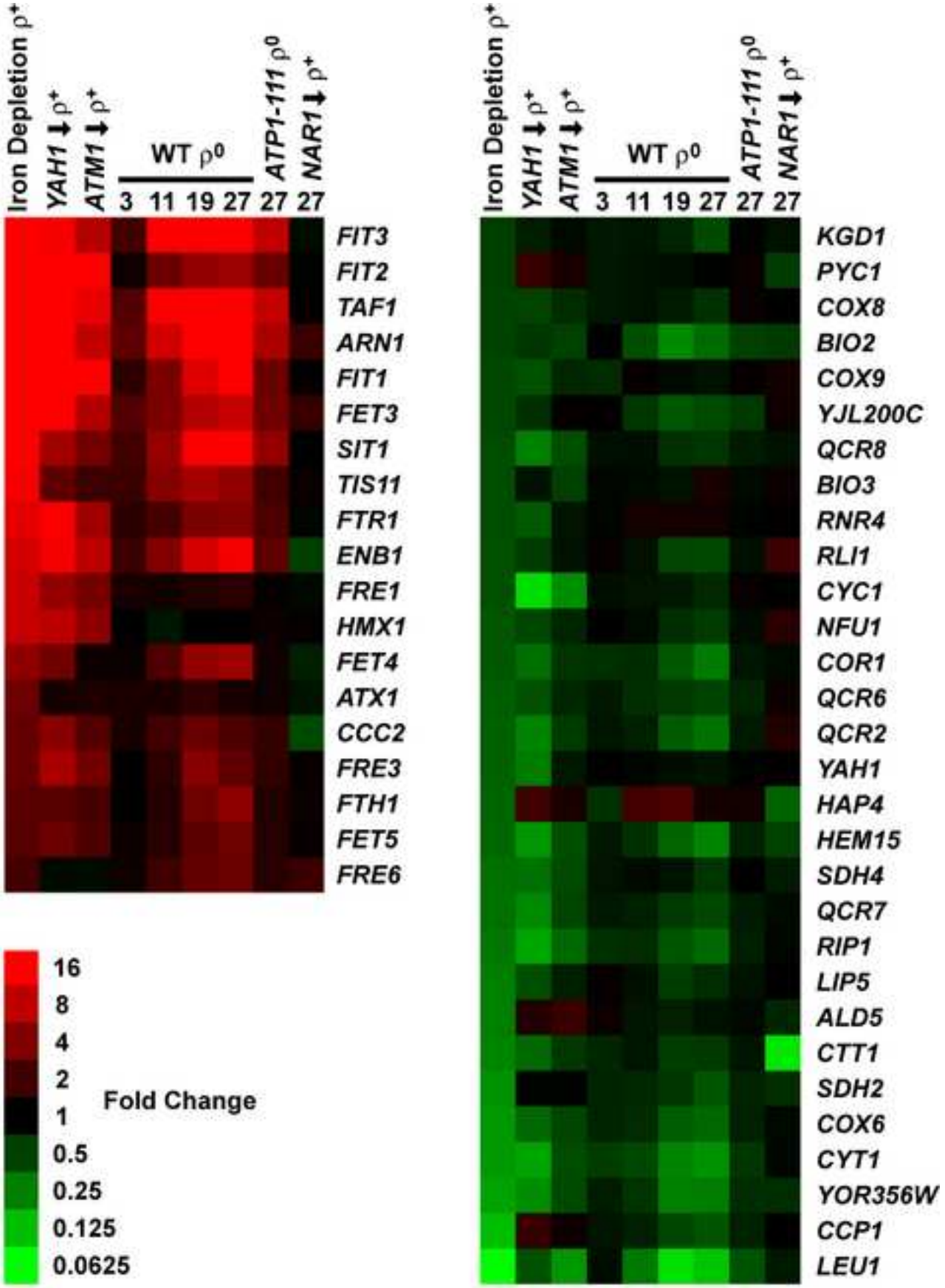

Figure 5

Figure 6

Click here to download high resolution image

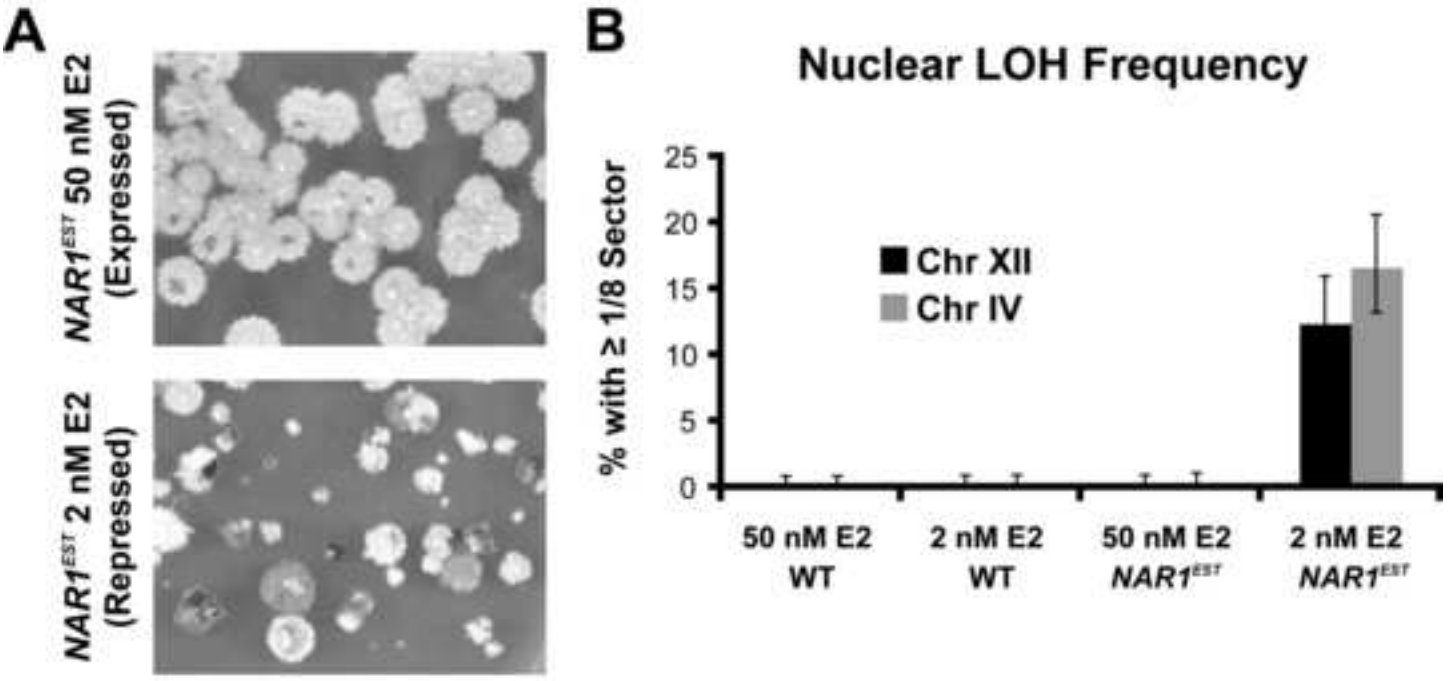

Figure 6

Figure 7

Click here to download high resolution image

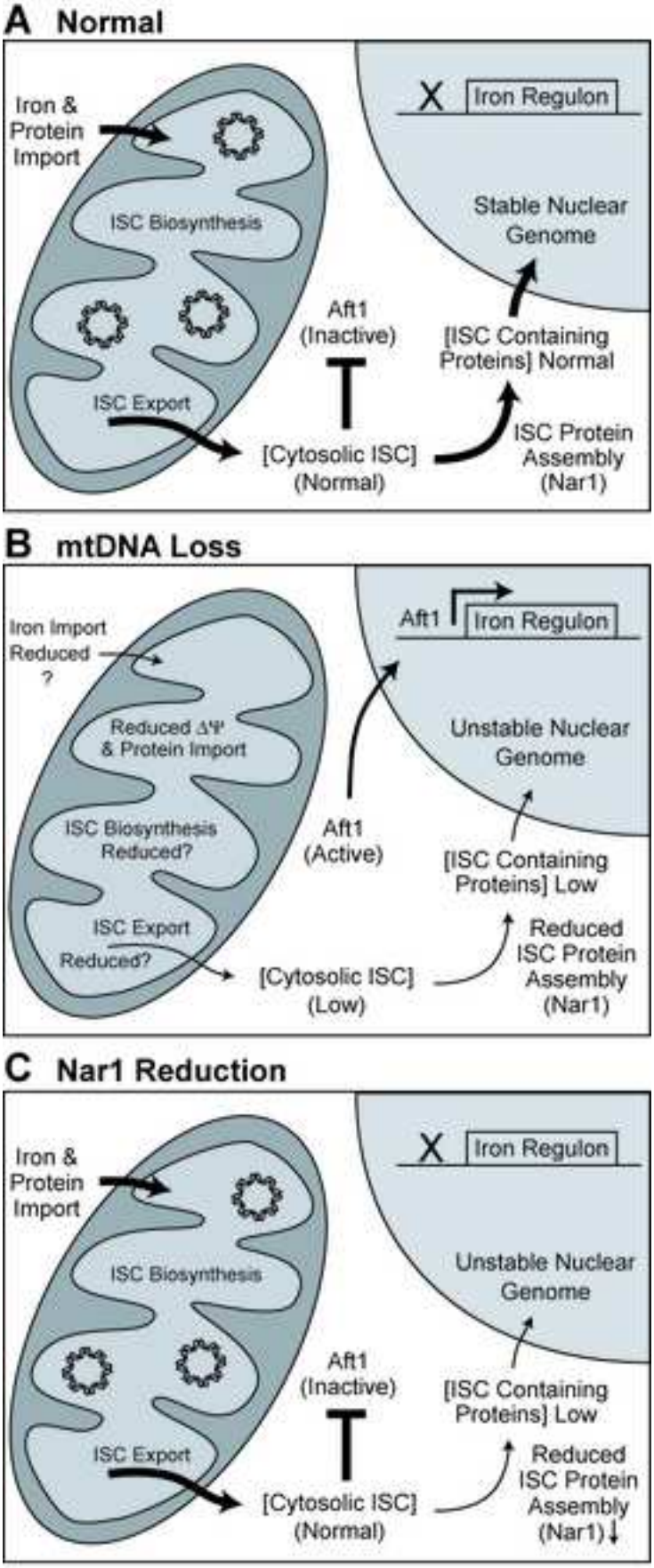

Figure 7

Supplemental Figure S1

Click here to download high resolution image

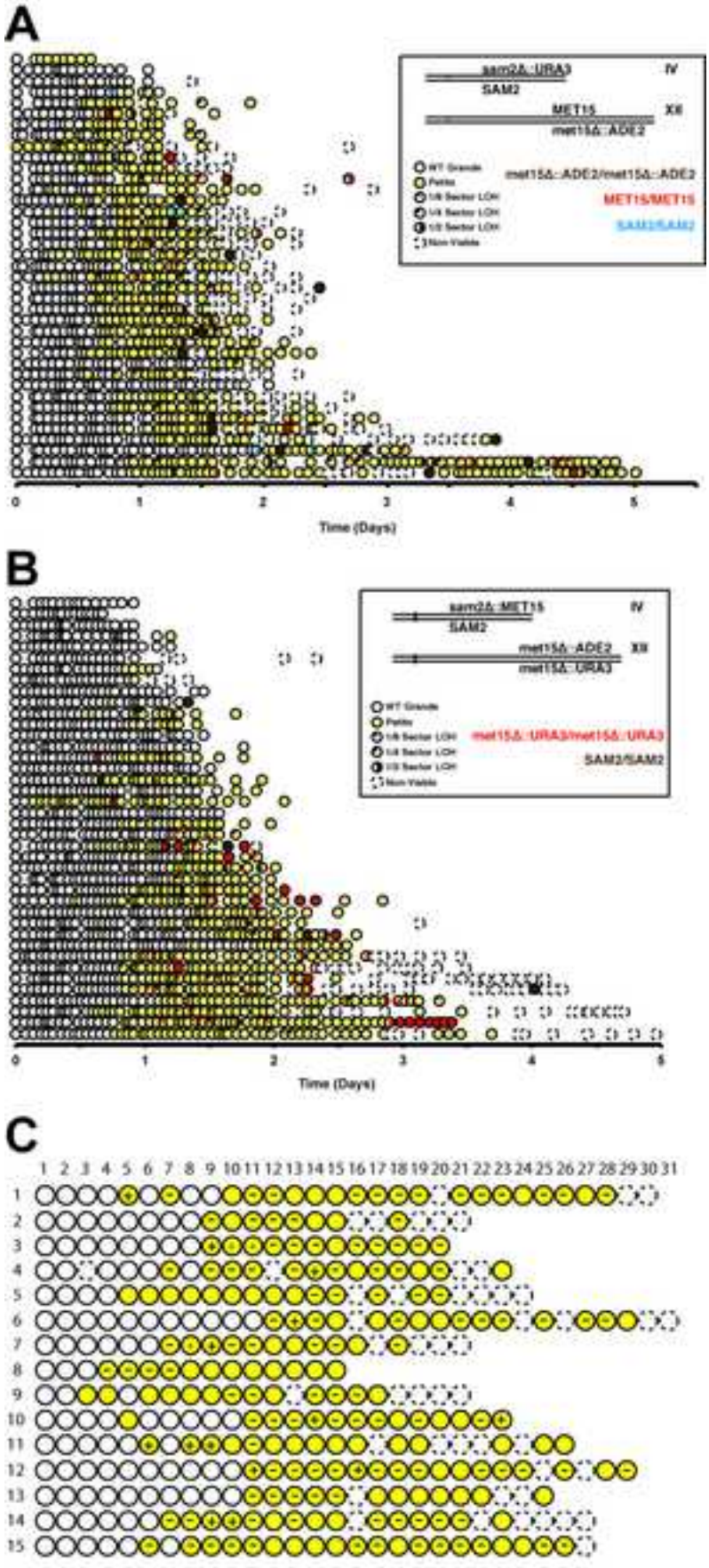

Figure S1

Supplemental Figure S2

Click here to download high resolution image

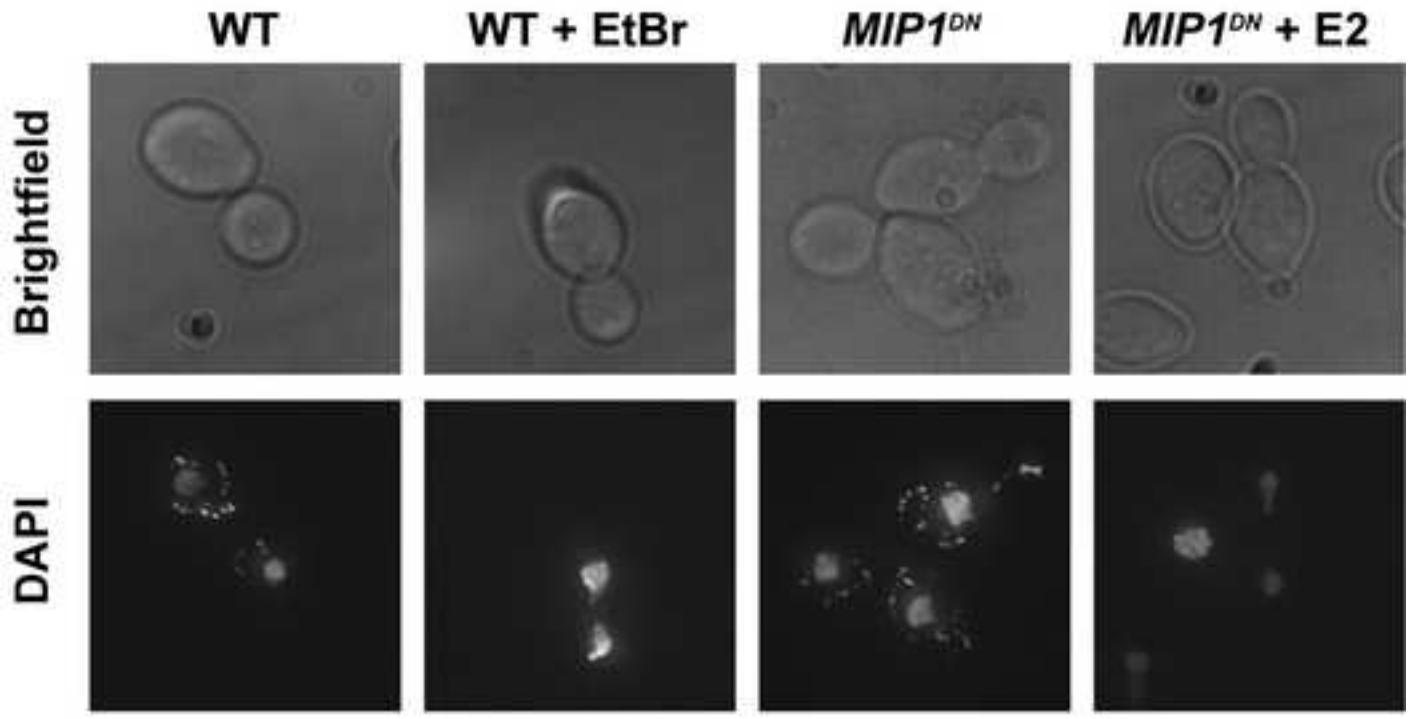

Figure S2

Supplemental Figure S3

Click here to download high resolution image

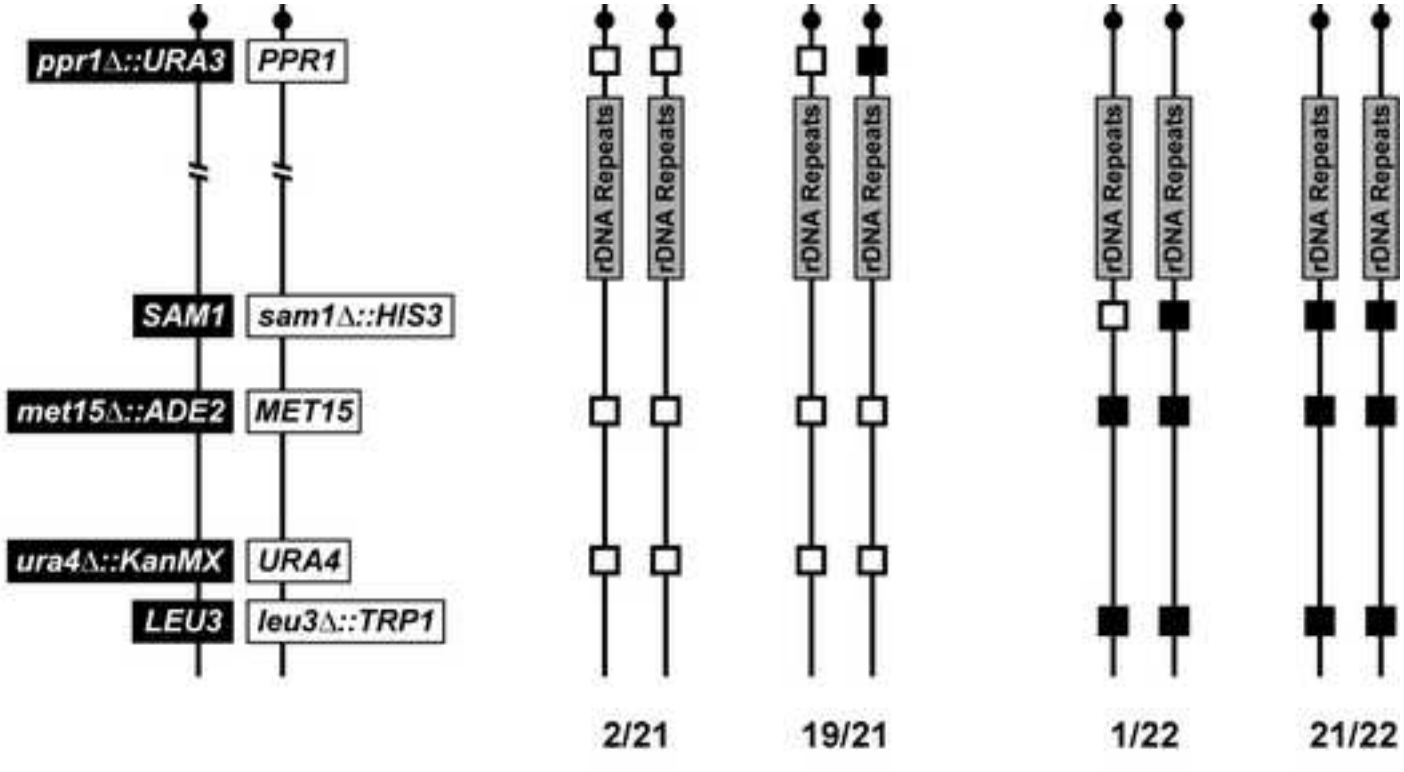

Figure S3

Supplemental Figure S4

Click here to download high resolution image

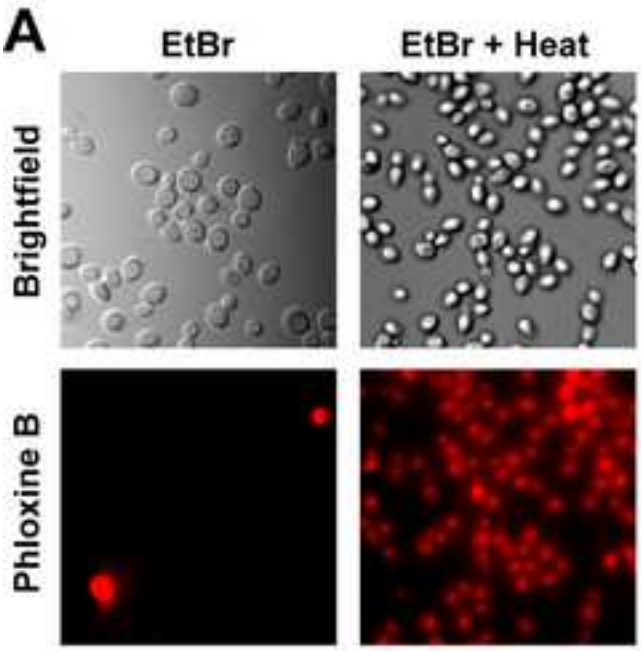

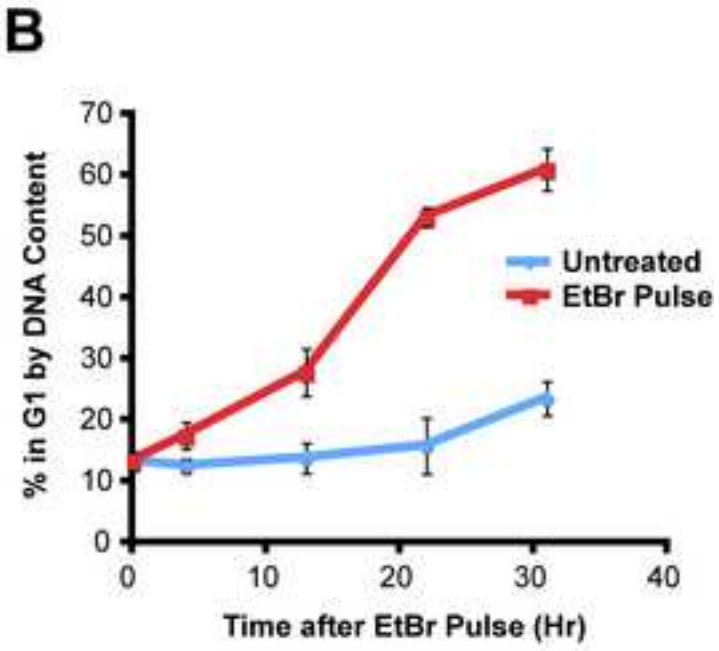

Figure S4

Supplemental Figure S5

Click here to download high resolution image

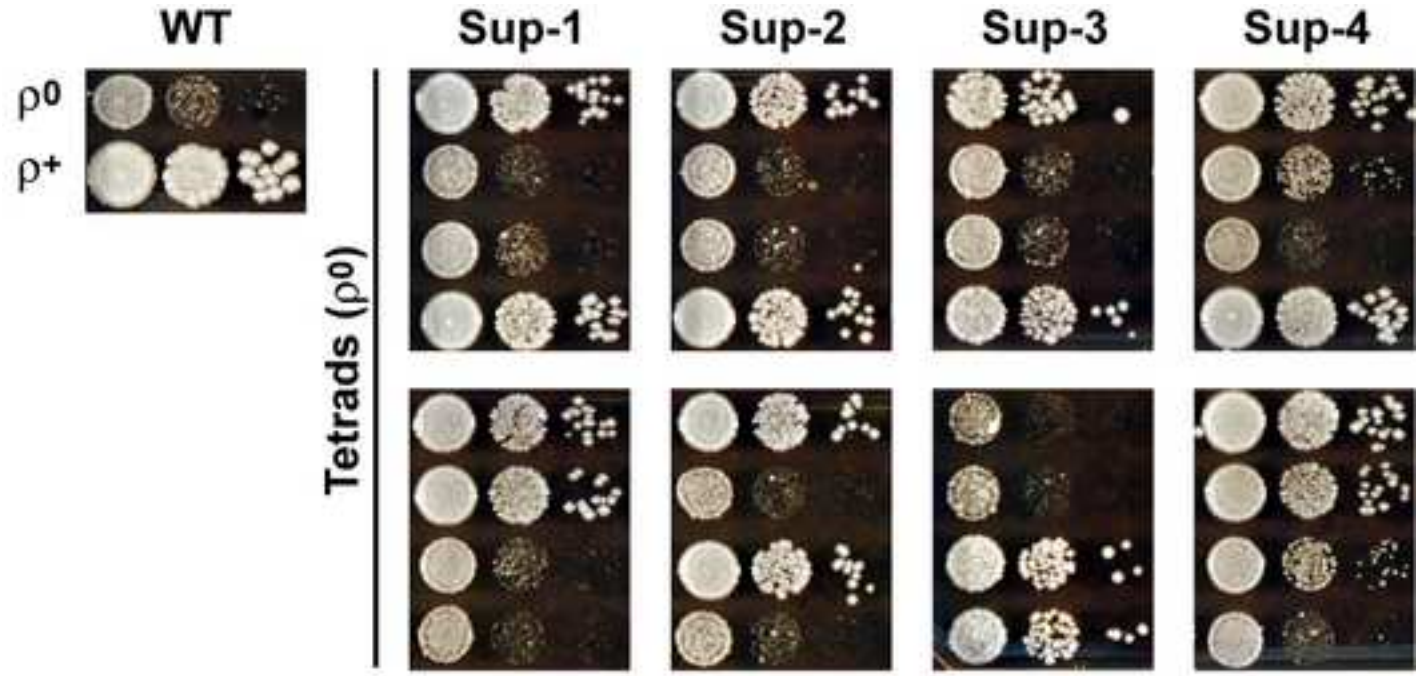

Figure S5

Supplemental Figure S6

Click here to download high resolution image

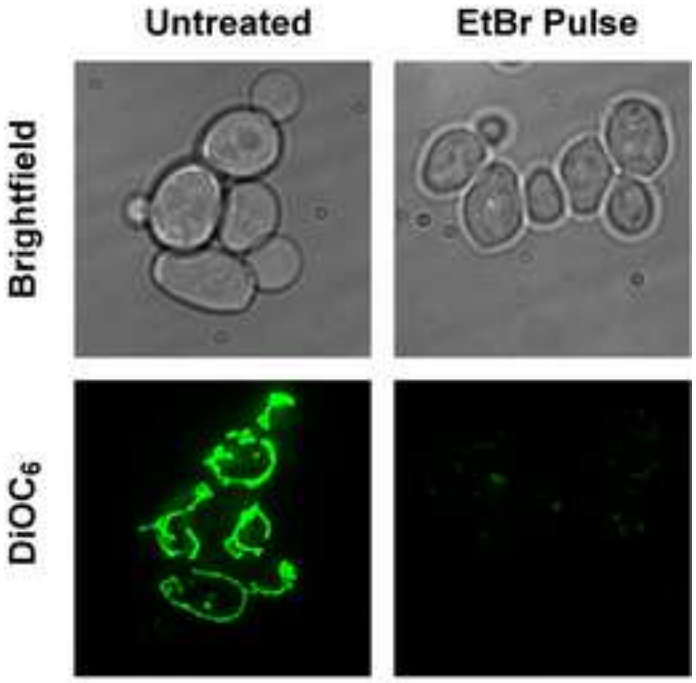

Figure S6

Supplemental Figure S7

Click here to download high resolution image

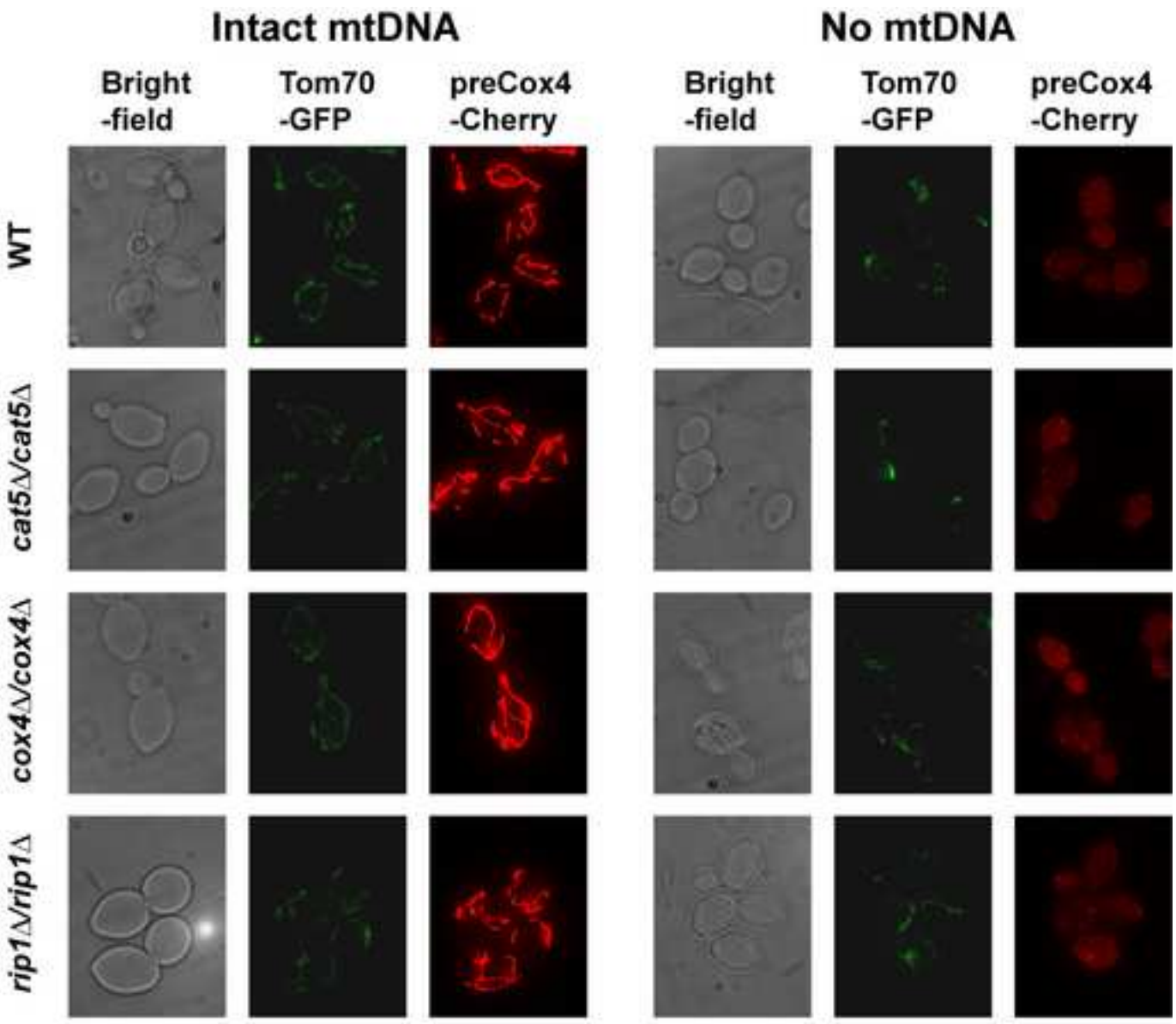

Figure S7

Supplemental Figure S8

Click here to download high resolution image

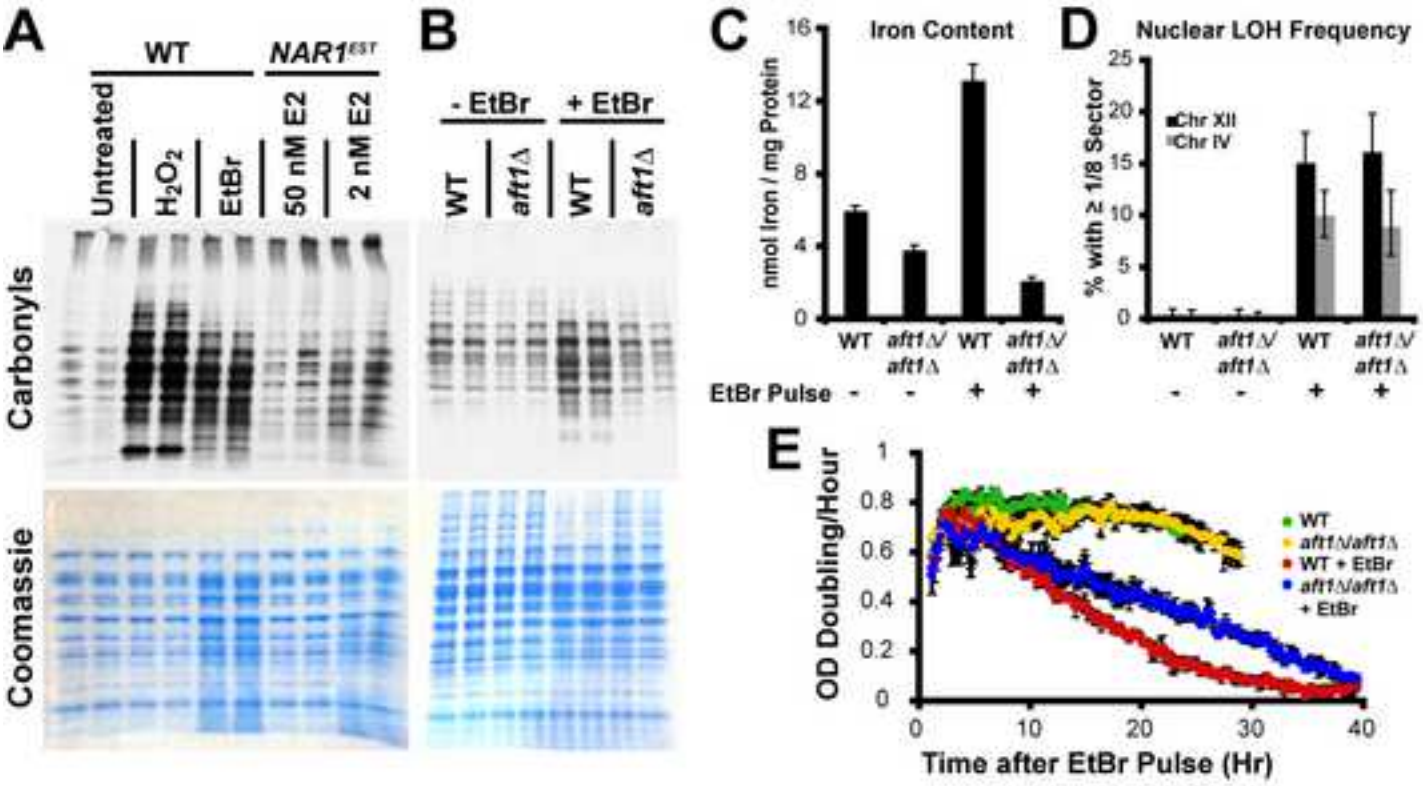

Figure S8

Supplemental Figure S9

Click here to download high resolution image

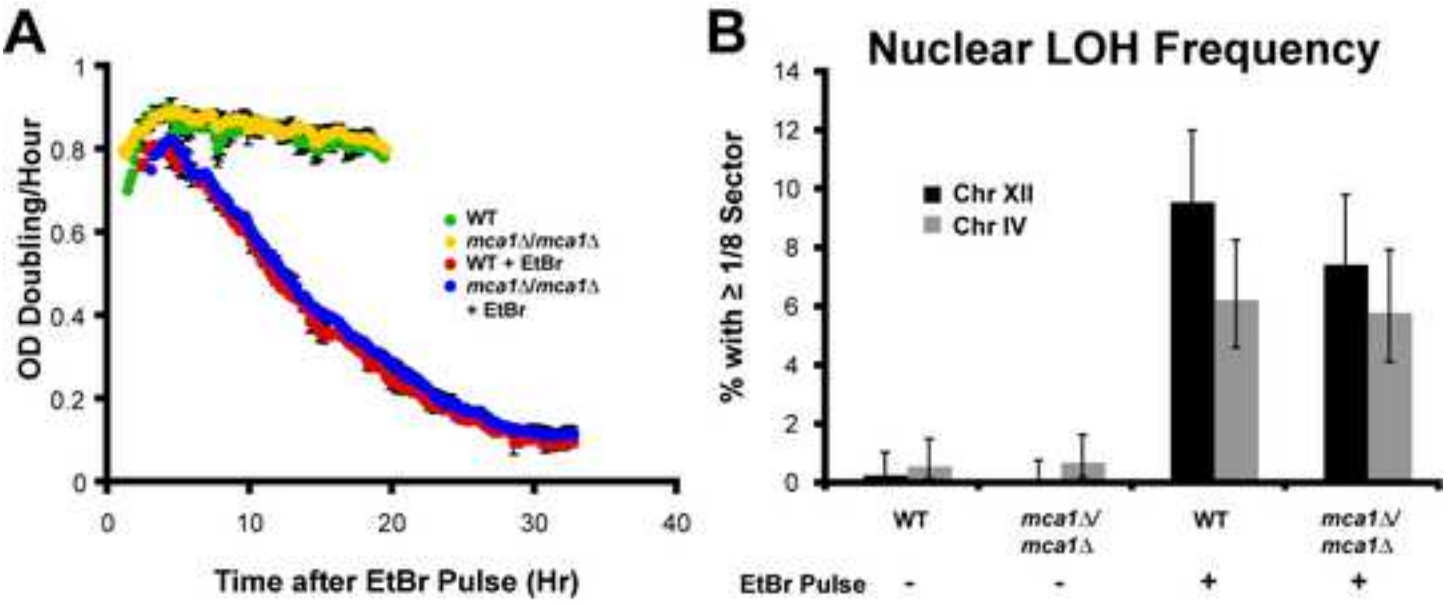

Figure S9

Table S1

Click here to download [H] Supplemental Movies and Spreadsheets: Table S1.xls

Supplemental tables S2 & S3

Click here to download [G] Supplemental Text and Figures: Table S2 S3 Strain Oligo.doc

Table S2. List of Yeast Strains Used in this Study

STRAIN	GENOTYPE	SOURCE
BY4743	*MAT***a**/*MATα his3Δ1/his3Δ1 leu2Δ0/leu2Δ0 ura3Δ0/ura3Δ0 met15Δ0/+ lys2Δ0/+*	(Brachmann et al., 1998)
BY4741	*MAT***a** *his3Δ1 leu2Δ0 met15Δ0 ura3Δ0*	(Brachmann et al., 1998)
BY4742	*MATα his3Δ1 leu2Δ0 lys2Δ0 ura3Δ0*	(Brachmann et al., 1998)
UCC809	*MAT***a**/*MATα ade2Δ::hisG/ade2Δ::hisG leu2Δ0/leu2Δ0 lys2Δ0/lys2Δ0 met15Δ::ADE2/met15Δ::URA3 trp1Δ63/trp1Δ63 ura3Δ0/ura3Δ0 arg8Δ::LEU2/+ gdh1d::LYS2/+ sam2d::MET15/+ ho/hoΔ::TRP1*	(McMurray and Gottschling, 2003)
UCC793	*MAT***a**/*MATα ade2Δ::hisG/ade2Δ::hisG leu2Δ0/leu2Δ0 lys2Δ0/lys2Δ0 trp1Δ63/trp1Δ63 ura3Δ0/ura3Δ0 sam2Δ::URA3/+ met15Δ::ADE2/+ arg8Δ::LEU2/+ gdh1Δ::LYS2/+*	(McMurray and Gottschling, 2003)
UCC1726	*MAT***a**/*MATα his3Δ1/his3Δ1 ura3Δ0/ura3Δ0 ade2Δ::hisG/ade2Δ::hisG lys2Δ0/lys2Δ0 leu2Δ0/leu2Δ0 met15Δ::ADE2/met15Δ::LYS2 chrIV(1515634-1515738)::SpHIS5/chrIV(1515634-1515738)::MET15*	This study
UCC1899	UCC1726 *RAD52-eGFP-KanMX/RAD52-eGFP-KanMX*	This study
UCC1924	UCC1726 *RAD52-eGFP-KanMX/RAD52-eGFP-KanMX leu2Δ0::pACT1-GAL4dbd-ER-VP16ad-NatMX/ leu2Δ0::pACT1-GAL4dbd-ER-VP16ad-NatMX hoΔ::URA3-pGAL1-MIP1^{DN}/hoΔ::URA3-pGAL1-MIP1^{DN}*	This study
UCC1932	UCC1726 *RAD52-eGFP-KanMX/RAD52-eGFP-KanMX leu2Δ0::pACT1-GAL4dbd-ER-VP16ad-NatMX/leu2Δ0::pACT1-GAL4dbd-ER-VP16ad-NatMX*	This study
UCC3818	UCC1726 *RAD52-eGFP-KanMX/RAD52-eGFP-KanMX cat5Δ::LEU2/cat5Δ::LEU2*	This study
UCC3820	UCC1726 *RAD52-eGFP-KanMX/RAD52-eGFP-KanMX rip1Δ::LEU2/rip1Δ::LEU2*	This study
UCC3822	UCC1726 *RAD52-eGFP-KanMX/RAD52-eGFP-KanMX cox4Δ::LEU2/cox4Δ::LEU2*	This study
UCC3857	UCC1726 *RAD52-eGFP-KanMX/RAD52-eGFP-KanMX mca1Δ::LEU2/mca1Δ::LEU2*	This study
UCC3863	UCC1726 *RAD52-eGFP-KanMX/RAD52-eGFP-KanMX rtg1Δ::URA3/rtg1Δ::URA3*	This study
UCC3970	UCC1726 *RAD52-eGFP-KanMX/RAD52-eGFP-KanMX leu2Δ0::* P$_{ACT1}$*-GAL4dbd-ER-VP16ad-NatMX/ leu2Δ0::*P$_{ACT1}$*-GAL4dbd-ER-VP16ad-NatMX URA3-*P$_{GAL1}$*-NAR1/URA3-* P$_{GAL1}$*-NAR1*	This study
UCC3980	UCC1726 *ATP1-111/ATP1-111*	This study
UCC3992	UCC1726 *TOM70-eGFP-CaURA3/+ chrIV(446393-446394)::*P$_{TDH3}$*-preCOX4-Cherry-hphMX/+*	This study
UCC3994	UCC1726 *ATP1-111/ATP1-111 TOM70-eGFP-CaURA3/+ chrIV(446393-446394)::*P$_{TDH3}$*-preCOX4-Cherry-hphMX/+*	This study
UCC3996	UCC1726 *TOM70-eGFP-KanMX/+ cat5Δ/cat5Δ chrIV(446393-446394)::*P$_{TDH3}$*-preCOX4-Cherry-hphMX/+*	This study
UCC3997	UCC1726 *TOM70-eGFP-KanMX/+ rip1Δ/rip1Δ chrIV(446393-446394)::*P$_{TDH3}$*-preCOX4-Cherry-hphMX/+*	This study
UCC3998	UCC1726 *TOM70-eGFP-KanMX/+ cox4Δ/cox4Δ chrIV(446393-446394)::*P$_{TDH3}$*-preCOX4-Cherry-hphMX/+*	This study
UCC3999	UCC1726 *aft1Δ::hphMX/aft1Δ::hphMX*	This study

Brachmann, C. B., Davies, A., Cost, G. J., Caputo, E., Li, J., Hieter, P., and Boeke, J. D. (1998). Designer deletion strains derived from Saccharomyces cerevisiae S288C: a useful set of strains and plasmids for PCR-mediated gene disruption and other applications. Yeast *14*, 115-132.

McMurray, M. A., and Gottschling, D. E. (2003). An age-induced switch to a hyper-recombinational state. Science *301*, 1908-1911.

Table S3. List of Oligonucleotides Used in this Study

OLIGO NAME	SEQUENCE
pACT1-AscI	GTACGGCGCGCCGCCTCTACCTTGCAGACCCATATAATA
pACT1-ApaI	GTACGGGCCCTGTTAATTCAGTAAATTTTCGATCTTGG
leu2d0-int1-PmeI	GCTTCCAAGACACACTTGGTTTAAACACAGAGTACTTTATACGTAC
leu2d0-int2-NotI	GATCGCGGCCGCATGATTAGAGGTCAAGAGGGCT
leu2d0-int3-SacII	GATCCCGCGGCGACACGAAATTACAAAATGGA
leu2d0-int4-PmeI	GTATAAAGTACTCTGTGTTTAAACCAAGTGTGTCTTGGAAGCCG
mip1-5-SpeI-2	TAGCACTAGTTAGTTGTTGAGCAACGAGGGA
mip1-3-SalI	TAGCGTCGACCAAATGCGAAAGCTAATGCAG
mip1-D918A-1	CATTTCCATCCATGCTGAGATTAGATTTTTG
mip1-D918A-2	CAAAAATCTAATCTCAGCATGGATGGAAATG
Hocre-R	ATGCTTTCTGAAAACACGACTATTCTGATGGCTAACGGTGAAAGATTGTACTGAGAGTGC
Hocre-F	GCAGATGCGCGCACCTGCGTTGTTACCACAACTCTTATGAGGTGATTACGCCAAGCGCGC
5'pnar1-1	ATTAAGAGAGCAGGTGACTTTCTGG
5'pnar1-2	GTATGGTGCACTCTCAGTACAATCGCTTTCTTGTACACTTATCTTGTCACT
pGAL1-F1	AATCAAGTTTTTTGGGGTCG
URA3-F1	TTTCCCCGTCAAGCTCTAAA
pGAL1-pTCG-up	TCGAGGAATTCGGCTAGAGGT
pRS+	GATTGTACTGAGAGTGCACC
3'pnar1-1	AACCTCTAGCCGAATTCCTCGAATGAGTGCTCTACTGTCCGAGTCT
3'pnar1-2	CTCCAATGTTAAGCCGTAGTACTG
atp1d5	CAGGCTGAAGAATTGGTCGAGTTCTCCTCTGGTGTTAAAGGTATGGCGATTGTACTGAGAGTGCACC
atp1d3	CCATCCAAATGACCATTAACACCGGCATAAATCAATGGAACCTGTTCCTGTGCGGTATTTCACACCG
CAT5rs1	ACGGGATTTTCAGGAAAAAAAACAATAGAAATCTATAAAACAGATTGTACTGAGAGTGCAC
CAT5rs2	CTGGCATAACGCGACTGATGTATGCCACTTTCTGGTGGTTACTGTGCGGTATTTCACACCG
gfp-rec1	CACTATTTGAAAGGTTTATCAATGCTTAAAACCTAGTTACGCAGTTCGAGTTTATCATTATCAATACTG
mitored-1	GTGGCTGGCTTGAAAAATCTTATAGATTGACGTAGTGAAAGCATTTTGTTTGTTTATGTGTGTTTATTCG
mitored-2	AGATTTTTCAAGCCAGCCACAAGAACTTTGTGTAGCTCTGGTCGACGGATCCCCGGG
mitored-3	ATATGCATCAGCTTATTGGGTCCACCAAGAAATCCCCTCGGATCGATGAATTCGAGCTCG
TOM70F5	TCAAGAAACTTTAGCTAAATTACGCGAACAGGGTTTAATGGGTGACGGTGCTGGTTTA
TOM70R3	TTTGTCTTCTCCTAAAAGTTTTTAAGTTTATGTTTACTGTTCGATGAATTCGAGCTCG
aft1d5	CTACGACAATGGAAGGCTTCAATCCGGCTGACATAGAACATGCGTCACCGGATTGTACTGAGAGTGCACC
aft1d3	CATCTATATGCTAATCTTCTGGCTTCACATACTTCAACTCGCCGTTCACCTGTGCGGTATTTCACACCG
cox4d5	CACCCATTTCGATTTTGATGTTGCCATACAAATAGATAACAAGCACAGATTGTACTGAGAGTGCACC
cox4d3	GTAAAAGAGAAACAGAAGGGCAACTTGAATGATAAGATTAGTGATGGCTGTGCGGTATTTCACACCG
rip1d5	CACTCTAACACTTATTAGGAAACCGAAAGGAGCAATAACAAACGATTGTACTGAGAGTGCACC
rip1d3	GACAATAAAGATGTAGTTTTCGAGGACGAAAAACAAACCTAACCAACCTGTGCGGTATTTCACACCG

SUPPLEMENTAL EXPERIMENTAL PROCEDURES

Strain and plasmid construction

All strains used in this study and their genotypes are presented in Table S2 and all oligonucleotides used in plasmid and strain constructions are listed in Table S3.

The Gal4-estrogen binding domain-VP16 (GEV) fusion protein was integrated at the genomic *leu2Δ0* allele by transforming the plasmid pAGL linearized with the restriction enzyme *Pme*I. This plasmid was created in three steps. First, pGEV-LEU2, which was a generous gift of Jennifer Pinkham (Gao and Pinkham, 2000), was partially digested with *Hind*III and *Not*I, and the fragment containing the GEV was cloned into a *Not*I/*Hind*III digested pRS40NAT (Andersen et al., 2008) to create plasmid pLND24 (a gift of Lazar Dimitrov – Gottschling lab). Next a genomic fragment containing the *ACT1* promoter amplified with the primers pACT1-apaI and pACT1-ascI were cloned between the *Apa*I and *Asc*I sites of pLND24 to make pACT1-GEV. Finally, a fusion PCR product between the following two fragments made using a genomic template: (1) primers leu2d0-int1-pmeI and leu2d0-int2-notI (2) primers leu2d0-int3-sacII and leu2d0-int4-pmeI was generated and cloned into the *Not*I and *Sac*II sites of pACT1-GEV.

The *MIP1* dominant negative allele was modeled after a dominant negative allele of the mammalian homolog, DNA polymerase γ (Jazayeri et al., 2003); the catalytic aspartic acid 918 residue was replaced with alanine. This allele was created by fusion PCR using the primers mip1-5-spe1-2, Mip1-D918A-1, Mip1-D918A-2, and mip1-3-sal1 and the template pFL39-MIP1, which was a generous gift of Francoise Foury (Foury, 1989). This fragment was cloned between the *Spe*I and *Sac*I sites of p416-*GAL1*

(Mumberg et al., 1994), and integrated at the *HO* locus using the primers HOcre-F and HOcre-R.

The *GAL1* promoter was inserted in front of the genomic *NAR1* gene by transformation with a fusion PCR made from the following 4 fragments: (1) primers 5'pnar1-1 and 5'pnar1-2, using genomic DNA as a template; (2) primers pRS+ and URA3-F1, using pRS306 as a template (Brachmann et al., 1998); (3) primers pGAL1-F1 and pGAL1-pTCG-up, using pTCG as a template (Singer et al., 1998); (4) primers 3'pnar1-1 and 3'pnar1-2, using genomic DNA as a template.

The *ATP1-111* allele was integrated by first replacing nucleotides 250-1475 of the *ATP1* gene with *URA3* using a PCR product made from the primers atp1d5 and atp1d3 using pRS306 as a template, followed by transformation of this strain with the *Xba*I/*Bam*HI fragment from pRS316-ATP1-111 and selection for strains that had lost the *URA3* marker. The plasmid pRS316-ATP1-111 was a generous gift from Peter Thorsness (Francis et al., 2007).

The plasmid pBS35 containing the mCherry gene was provided by Roger Tsien (UCSD) through the Yeast Resource Center (Seattle, WA). The heterochimeric fusion protein between the pre-sequence of *COX4* and the mCherry protein was put under the control of the *TDH3* promoter and integrated at an intergenic region near the centromere of chromosome IV by transforming a fusion PCR from primers gfp-rec1 and mitored1 using genomic DNA as a template and primers mitored2 and mitored3 with pBS35 as a template. One transformant that showed reduced expression and more mitochondria-specific localization was used for all subsequent experiments.

Plasmids pKT209 and pKT127 (Sheff and Thorn, 2004) were used as template to fuse the enhanced green fluorescent protein to the 3' end of the genomic copy of *TOM70* using the primers TOM70F5 and TOM70R3.

Strains with gene deletions were generated by PCR-mediated gene replacement by homologous recombination (see Table S3 for oligos used). Diploids homozygous for a given deletion were either created by knocking out one copy of the gene in a diploid cell, followed by sporulation, and mating the haploid strains carrying the deletion, or by knocking out each gene in the haploid parents, and subsequent mating.

Growth rate measurements

Growth rates of cultures were measured by optical density at 660 nm in 96-well plates using a Powerwave XS plate reader (BioTek, Winooski, VT) using a modification of the method reported previously (Toussaint and Conconi, 2006). In order to follow the growth rate of the same culture for a long period of time, a series of seven 4-fold dilutions of each original culture were made in final volumes of 100 µl. The plate was grown at 30° with high, continuous shaking for 24-40 hours with absorbance reads every 10 minutes. Growth rates of individual wells were calculated when the path length-unadjusted absorbance for that well was between 0.02 and 0.25, and the doubling time was calculated by linear regression of the $\log_2$ transformed OD using a 110 minute sliding window. Individual wells representing different dilutions of the same culture were subsequently averaged together when they both were in the required window. In each experiment, each curve represents the mean of at least 3 independent cultures, plus or minus the standard deviation.

Supplemental microscopy

$DiOC_6$ staining of live cells was performed as previously described (Pringle et al., 1989) in synthetic complete medium with a concentration of 250 ng/ml $DiOC_6$ (Molecular probes), using the FITC filter and an exposure time of 0.2 sec, taking 12 z-slices 0.5 µm apart, and projecting these z-slices onto a single plane using the brightest point. Images were false colored using ImageJ software (v1.37, NIH).

Iron level assay

Fifty ml cultures were grown as described to an OD_{600} 0.6 - 1.2. Cells were washed 2 times with 50 ml nanopure water, and suspended in an equal volume of sample buffer (adapted from (Aguilaniu et al., 2001)):(20 mM Tris-Cl, pH 8, 10 mM $MgCl_2$, 0.33 M ammonium sulfate, 5% glycerol, 1X Roche protease inhibitor cocktail, 1% 2-mercaptoethanol) with Triton X-100 added to a final concentration of 0.5%. The cells were stored at -20°, thawed and lysed by vortexing with glass beads in a multi-vortexer for 30 min at 4°. Protein levels were quantified using the Biorad protein quantitation kit, and iron levels were measured using the acid extraction and chelation method using 2-(5-nitro-2-pyridylazo)-5-(N-propyl-N-sulfopropylamino)phenol (Nitro-PAPS) as previously described (Molik et al., 2007). Iron levels are reported as the mean of three independent replicates, with error bars representing the standard error of the mean.

Protein carbonylation assay

Cultures were grown as described above to an OD_{600} of 1 in biological duplicate, and were disrupted in sample buffer. Identical amounts of total protein were then derivatized and detected using the Oxyblot™ protein oxidation detection kit (Chemicon International) using the manufacturer's instructions.

DNA content analysis

DNA of cells fixed in 70% ethanol were stained with SYTOX Green (Invitrogen), as previously described (Foss, 2001), and DNA content was measured using a BD FACSCanto flow cytometer (BD Biosciences) and cell cycle profiles were analyzed using FlowJo software (Tree Star Inc.).

REFERENCES FOR SUPPLEMENTAL EXPERIMENTAL PROCEDURES

Aguilaniu, H., Gustafsson, L., Rigoulet, M., and Nystrom, T. (2001). Protein oxidation in G0 cells of Saccharomyces cerevisiae depends on the state rather than rate of respiration and is enhanced in pos9 but not yap1 mutants. J Biol Chem *276*, 35396-35404.

Andersen, M.P., Nelson, Z.W., Hetrick, E.D., and Gottschling, D.E. (2008). A genetic screen for increased loss of heterozygosity in Saccharomyces cerevisiae. Genetics *179*, 1179-1195.

Brachmann, C.B., Davies, A., Cost, G.J., Caputo, E., Li, J., Hieter, P., and Boeke, J.D. (1998). Designer deletion strains derived from Saccharomyces cerevisiae S288C: a useful set of strains and plasmids for PCR-mediated gene disruption and other applications. Yeast *14*, 115-132.

Foss, E.J. (2001). Tof1p regulates DNA damage responses during S phase in Saccharomyces cerevisiae. Genetics *157*, 567-577.

Foury, F. (1989). Cloning and sequencing of the nuclear gene MIP1 encoding the catalytic subunit of the yeast mitochondrial DNA polymerase. J Biol Chem *264*, 20552-20560.

Francis, B.R., White, K.H., and Thorsness, P.E. (2007). Mutations in the Atp1p and Atp3p subunits of yeast ATP synthase differentially affect respiration and fermentation in Saccharomyces cerevisiae. J Bioenerg Biomembr *39*, 127-144.

Gao, C.Y., and Pinkham, J.L. (2000). Tightly regulated, beta-estradiol dose-dependent expression system for yeast. Biotechniques *29*, 1226-1231.

Jazayeri, M., Andreyev, A., Will, Y., Ward, M., Anderson, C.M., and Clevenger, W. (2003). Inducible expression of a dominant negative DNA polymerase-gamma depletes mitochondrial DNA and produces a rho0 phenotype. J Biol Chem *278*, 9823-9830.

Molik, S., Lill, R., and Muhlenhoff, U. (2007). Methods for studying iron metabolism in yeast mitochondria. Methods Cell Biol *80*, 261-280.

Mumberg, D., Muller, R., and Funk, M. (1994). Regulatable promoters of Saccharomyces cerevisiae: comparison of transcriptional activity and their use for heterologous expression. Nucleic Acids Res *22*, 5767-5768.

Pringle, J.R., Preston, R.A., Adams, A.E., Stearns, T., Drubin, D.G., Haarer, B.K., and Jones, E.W. (1989). Fluorescence microscopy methods for yeast. Methods Cell Biol *31*, 357-435.

Sheff, M.A., and Thorn, K.S. (2004). Optimized cassettes for fluorescent protein tagging in Saccharomyces cerevisiae. Yeast *21*, 661-670.

Singer, M.S., Kahana, A., Wolf, A.J., Meisinger, L.L., Peterson, S.E., Goggin, C., Mahowald, M., and Gottschling, D.E. (1998). Identification of high-copy disruptors of telomeric silencing in Saccharomyces cerevisiae. Genetics *150*, 613-632.

Toussaint, M., and Conconi, A. (2006). High-throughput and sensitive assay to measure yeast cell growth: a bench protocol for testing genotoxic agents. Nat Protoc *1*, 1922-1928.

SUPPLEMENTAL FIGURE & TABLE LEGENDS

Figure S1: mtDNA instability and loss of heterozygosity in pedigree analysis

(A) Representation of pedigree analysis of forty mothers of the strain UCC809 arranged on the y-axis. Circles represent daughter colonies, yellow color indicates "petite" non-respiring colonies, red and black colored sectors in colonies represent LOH events at *met15*Δ*::ADE2* and *sam2*Δ*::MET15*, respectively. Dashed circles represent daughters that did not form visible colonies. (B) Representation of pedigree analysis of forty mothers of the strain UCC793 arranged on the y-axis. Circles represent daughter colonies, yellow color indicates "petite" non-respiring colonies, brown, red and blue colored sectors in colonies represent LOH events at *MET15*, *met15*Δ*::ADE2* and *sam2*Δ*::URA3*, respectively. Dashed circles represent daughters that did not form visible colonies. (C) 15 mothers from the wild-type strain UCC809 were analyzed by pedigree analysis. A sample of 128 non-respiring daughter colonies from these 15 pedigrees were stained with DAPI and scored for the presence or absence of cytoplasmic speckles, corresponding to the presence of mtDNA. The 15 mother cells are arranged on the y-axis, with each circle representing one daughter colony. Yellow circles represent "petite" non-respiring colonies. Colonies marked with a (+) have a fraction of cells with mtDNA staining. Colonies marked with a (-) showed no mtDNA staining. Dashed circles represent daughter cells that did not form visible colonies.

Figure S2: Treatment with Ethidium Bromide or induction of the *MIP1* dominant negative leads to rapid loss of the mtDNA. The wild-type strain (UCC1899) was grown in either the presence or absence of 30 µg/ml ethidium bromide for 7 hours. The strain

(UCC1924) containing the GEV transcriptional activator and the P_{GAL1}-$MIP1^{DN}$ allele was grown for 7 hours in the presence or absence of 1μM estradiol (E2). Following treatments, cells were fixed in paraformaldehyde, permeablized, and stained with DAPI to visualize the mitochondrial DNA.

Figure S3: Nuclear LOH following mtDNA loss occurs through mitotic recombination. A strain (UCC768), which contains multiple heterozygous markers on the right arm of chromosome XII was treated with ethidium bromide and plated to detect LOH events at the *MET15* locus (McMurray and Gottschling, 2003). Twenty-one clones that were homozygous for *MET15* (white box) and 22 that were homozygous for *met15*Δ*::ADE2* were subsequently phenotyped for the presence of other genetic markers along the chromosome arm (i.e. *URA3, HIS3, KanMX* and *TRP1*). The results are schematically presented.

Figure S4: Cells in the crisis following mtDNA loss are metabolically alive. (A) A wild-type strain (UCC1899) was transiently treated with ethidium bromide, grown without nutrient limitation for 30 hours, and stained for 5 minutes with 0.4 μg/ml of the vital dye phloxine B, and visualized by brightfield and a TRITC filter fluorescence microscopy. The same cells were heat killed by incubating 10 minutes at 65° and analyzed similarly. (B) The same strain was either transiently treated (red) or mock-treated (blue) with ethidium bromide and FACS analyzed for DNA content over time.

Figure S5: Spontaneous suppressors of the crisis following the loss of the mtDNA show Mendelian segregation. Spontaneous ρ^0 suppressors derived from the haploid wild-type strains BY4741 (sup-1, sup-2) and BY4742 (sup-3, sup-4) were backcrossed to a [ρ^+] wild-type parent and the resulting diploids were sporulated. Each [ρ^+] spore from each of two tetrads for these 4 mutants was transiently treated with ethidium bromide. Following treatment the cells were washed and three sequential 15-fold dilutions of each strain were placed onto plates and grown for 3 days. The upper left-hand panel contains a wild-type reference strain transiently treated with or without ethidium bromide.

Figure S6: Cells show reduced mitochondrial staining with the membrane potential sensitive dye $DiOC_6$ following loss of the mtDNA. A wild-type strain (UCC3992) was transiently treated with or without ethidium bromide, followed by 14 hours of growth in synthetic complete medium. Cells were stained with 250 ng/ml $DiOC_6$ in the same medium, placed onto a 2% agarose pad made of synthetic complete medium with 250ng/ml $DiOC_6$, and visualized using the FITC fluorescence filter or by brightfield microscopy.

Figure S7: Loss of respiratory function is not sufficient to impair mitochondrial matrix protein import. Localization of proteins to the outer mitochondrial membrane (Tom70-GFP, green) or the mitochondrial matrix (preCox4-Cherry, red) in wild-type (UCC3992), *cat5*Δ/*cat5*Δ, *cox4*Δ/*cox4*Δ or *rip1*Δ/*rip1*Δ cells are presented. Cells were grown for 15 hours following their transient treatment with (No mtDNA) or without (Intact mtDNA) ethidium bromide.

Figure S8: Increased cellular iron is not required for nuclear genomic instability following the loss of the mtDNA.

(A) Oxidation of soluble protein was determined by carbonyl analysis. Equal amounts of soluble cellular protein were loaded with two independent samples from the wild-type strain (UCC1899) grown in log phase, treated with 5mM hydrogen peroxide (H_2O_2) for 1 hour. The same strain was also treated with a 6-hour pulse of ethidium bromide, followed by 27 hours of growth. A derivative of this strain (UCC3970) with estradiol-controlled expression of the *NAR1* gene ($NAR1^{EST}$) protein was grown in 50 nM or 2nM estradiol (E2). A gel with the same samples coomassie stained for total protein is below. (B) The carbonyl analysis was repeated on a wild-type strain (UCC1726) and derivative containing a homozygous deletion of *AFT1* that were treated with or without a 6-hour pulse of ethidium bromide, followed by 24 hours of growth. The same cells described in (B) had their total cellular iron levels measured (C), the frequency of LOH determined (D), and their growth rate measured (E).

Figure S9: The yeast caspase Mca1 is not required for the crisis following mtDNA loss. (A) A wild-type strain (UCC1899) and its isogenic *mca1*Δ*/mca1*Δ derivative were transiently treated with or without ethidium bromide, and the growth rate was monitored as described in the Experimental Procedures. (B) The LOH frequency was determined for strains from (A) that were transiently treated ethidium bromide and plated following 8 hours of growth.

Table S1: Expression data:

RNA microarray data was analyzed with GeneSpring software (v.7 Agilent). Each

experiment was performed in biological triplicate. For the wild-type strain (UCC1899), samples were collected at each time point (hours) after the transient treatment of cells with ethidium bromide and compared to the parental strain with intact mtDNA. For the *ATP1-111* strain (UCC3980) cells were collected 27 hours after the ethidium bromide treatment, and compared to the same strain with intact mtDNA. For the *NAR1* reduced expression samples, UCC3970 was shifted from 50 nM to 2 nM estradiol, grown for 27 hours, and compared to the same strain grown in 50 nM estradiol. Dyes were exchanged for each biological replicate to rule out dye-specific artifacts. The numbers presented in this table are the mean of six hybridizations (2 dye-exchanges for each of 3 biological replicates) and the uncorrected t-test p values for each gene. Data points, which were changed at least 2-fold and achieved significance at a false discovery rate of 5% by the Benjamini-Hochberg multiple testing correction are shaded in blue.

A number of genes expression changed in response to shift of the estradiol-controlled *NAR1* strain (UCC3970) to low estradiol are also seen in a isogenic strain containing the GEV transcriptional activator but without the *GAL1* promoter controlling the *NAR1* gene (data not shown). These are primarily genes with Gal4 binding sites and were not included in our analysis. We have not seen significant transcriptional changes associated with different estradiol concentrations in the absence of the GEV (data not shown), indicating that the transcriptional changes observed are the result of the GEV induction.

REFERENCES FOR SUPPLEMENTAL FIGURES & TABLE

McMurray, M.A., and Gottschling, D.E. (2003). An age-induced switch to a hyper-recombinational state. Science *301*, 1908-1911.